Mucins shed from the laminated layer in cystic echinococcosis are captured by Kupffer cells via the lectin receptor Clec4F

Anabella A. Barrios[a], Camila Mouhape[a], Leonard Schreiber[b], Juliane Nell[b], Mariana Suárez-Martins[a], Geraldine Schlapp[c], María Noel Meikle[c], Ana Paula Mulet[c], Tsui-Ling Hsu[d], Shie-Liang Hsieh[d], Gustavo Mourglia-Ettlin[a], Carlos González[e], Martina Crispo[c], Thomas F. E. Barth[b], Cecilia Casaravilla[a], Stephen J. Jenkins[f] & Álvaro Díaz[a]

a. Área Inmunología, Departamento de Biociencias (Facultad de Química) and Cátedra de Inmunología, Instituto de Química Biológica (Facultad de Ciencias), Universidad de la República, Montevideo, Uruguay.
b. Institute of Pathology, University Ulm, Ulm, Germany
c. Unidad de Biotecnología en Animales de Laboratorio, Institut Pasteur de Montevideo, Montevideo, Uruguay.
d. Genomics Research Center, Academia Sinica, Taipei, Taiwan.
e. Retired from: CIMMYT (Centro Internacional de Mejoramiento de Maíz y Trigo), El Batán, México.
f. University of Edinburgh Centre for Inflammation Research, Queen's Medical Research Institute, University of Edinburgh, Edinburgh, UK.

Running title: Kupffer cells capture *Echinococcus* mucins via Clec4F

Corresponding author:

Full name: Álvaro Díaz

Department: Área Inmunología, Departamento de Biociencias (Facultad de Química) and Cátedra de Inmunología, Instituto de Química Biológica (Facultad de Ciencias), Universidad de la República, Montevideo, Uruguay.

Street address, city, postal code and country: Instituto de Higiene. Avenida Alfredo Navarro 3051. Montevideo CP 11600. Uruguay.

Tel: + 598 24874320

E-mail: adiaz@fq.edu.uy, alvarojdy@gmail.com

Keywords: *Echinococcus*, laminated layer, lectin, mucin, Kupffer cells, Clec4F

Abstract

Cystic echinococcosis is caused by the larval stages (hydatids) of cestode parasites belonging to the species cluster *Echinococcus granulosus sensu lato*. Hydatids are bladder-like structures that attain large sizes within various internal organs of livestock ungulates and humans. Hydatids are protected by the massive acellular laminated layer (LL), composed mainly by mucins. Parasite growth requires LL turnover, and abundant LL-derived particles are found at infection sites in infected humans, raising the question of how LL materials are dealt with by the hosts. In this article, we show that LL mucins injected into mice are taken up by Kupffer cells, the liver macrophages exposed to the vascular space. This uptake is largely dependent on the intact mucin glycans and on Clec4F, a C-type lectin receptor which in rodents is selectively expressed in Kupffer cells. This uptake mechanism operates on mucins injected both in soluble form i.v. and in particulate form i.p. In mice harbouring intraperitoneal infections, LL mucins were found essentially only at the infection site and in the liver, where they were taken up by Kupffer cells via Clec4F. Therefore, shed LL materials circulate in the host and Kupffer cells can act as a sink for these materials even when the parasite grows in sites other than the liver.

57 **Introduction**

58

59 The larval stages of the cestode parasites belonging to the species cluster known as
60 *Echinococcus granulosus sensu lato* (distinguishable only by molecular means) cause
61 cystic echinococcosis in livestock animals including sheep and cattle, as well as in
62 humans (1, 2). This disease is characterized by the growth within organ parenchymae of
63 bladder-like parasite structures called hydatids. Each hydatid is bounded by a thin cellular
64 layer, in turn protected by a thick acellular coat called the laminated layer (LL) (3–6).
65 The main component of the LL is a meshwork of mucins, heavily decorated by O-glycans
66 that are rich in galactose (7, 8). Hydatids persist in internal organs of immunocompetent
67 hosts for up to decades, and they usually elicit weak local inflammation (9). The growth
68 of the hydatid (potentially through over 3 orders of magnitude in lineal dimension)
69 requires the shedding of materials from the LL (3–6). In human infections, the abundant
70 shed LL particles (termed SPEGs, for shed particles of *E. granulosus*) are found in the
71 tissue surrounding the parasite and in the draining lymph nodes (10).

72

73 The persistence of larval *E. granulosus* infection, the massive nature of the LL, and sheer
74 abundance of shed particles as detected in human infection call the question of how the
75 host's body disposes of this foreign debris and avoids the potential inflammation that may
76 result from its build-up. As inflammation is detrimental to the parasite (9), it makes
77 biological sense that LL constituents may be evolutionarily perfected for engaging
78 cellular receptors that will ensure non-inflammatory disposal of the shed materials.

79

80 Studies on the responses elicited in mouse dendritic cells (DC) and macrophages by *in*
81 *vitro*-produced LL particles (pLL, from particulate LL) have suggested an interaction

82 mode independent of conventional receptors and inefficient phagocytosis, at least in the
83 absence of opsonization (6, 11, 12). In broad agreement, none out of 35 human innate
84 carbohydrate-recognition proteins (recombinantly expressed as fusions with IgG Fc)
85 bound the LL mucins in an *in vitro* screening (13). However, in the same experiment,
86 strong binding was observed for mouse Clec4F. This type II, trimeric, cell-surface C-type
87 lectin has affinity for glycans terminated in N-acetylgalactosamine or galactose (Gal),
88 especially when they occur in tandem along the same backbone, as it happens in mucins
89 (14–18). The binding of recombinant Clec4F to the LL mucins was as expected calcium-
90 dependent and resistant to digestion of non-mucin proteins in the parasite preparation.
91 Binding was also observed to a number of synthetic glycans representing some of the
92 main carbohydrate motifs in the *E. granulosus* LL and/or in the LL of the related species
93 *Echinococcus multilocularis* (13).
94
95 In rodents, Clec4F is exclusively expressed in Kupffer cells (KC) (14–16), the sessile
96 liver macrophages exposed to the vascular space. This restricted expression means that
97 Clec4F is not expressed in the mouse DC and macrophage sub-types used in the
98 previously mentioned experiments that suggested a receptor-independent interaction
99 mode with LL particles (6, 11, 12). In the ungulate natural hosts of *E. granulosus*, Clec4F
100 appears to be expressed in lymphoid tissues in addition to the liver (15). In humans,
101 Clec4F is not functional as a lectin and is poorly or not expressed (15).
102
103 The only demonstrated function of Clec4F (in mice) is the removal from circulation of
104 de-sialylated platelets by KC (19). Although the macrophage galactose-type lectins
105 (MGL) and the asialoglycoprotein receptor (ASGR; reported to be expressed in KC in

106 addition to in hepatocytes) collaborate in this function, Clec4F appears to fulfil an
107 indispensable role (19–21).
108
109 KC under basal conditions have a tolerogenic profile as antigen-presenting cells (22).
110 Also, a role of Clec4F in removing de-sialylated platelets (19), conceptually akin to the
111 role of the receptors involved in phagocytosis of apoptotic cells (23), suggests that Clec4F
112 is not wired to inflammatory responses. Thus, Clec4F/KC appears to be an evolutionary
113 option from the parasite's standpoint for LL debris disposal. However, *in vitro* binding
114 by the soluble Clec4F lectin domain expressed in dimeric form (13) does not predict
115 binding by the native cell-surface trimeric receptor, or internalization by KC. In this
116 article, we analyse *in vivo* uptake of soluble and particulate LL materials by KC and the
117 role of Clec4F in this process, in the context of artificial injection of materials as well as
118 experimental infection.
119
120 **Materials and Methods**
121
122 *Parasite materials*
123 The starting material for LL mucin preparations, and the source of protoscoleces for
124 experimental infections, were macroscopically healthy, fertile *E. granulosus sensu lato*
125 hydatids from natural infections in cattle from Uruguay. For LL mucin preparations,
126 hydatid walls, which have the LL as the overwhelmingly dominant component (3, 4, 8),
127 were extensively washed with phosphate-buffered saline (PBS), then with 2 M NaCl and
128 finally with water. The walls were then dehydrated by sequential steps with ethanol (95%
129 v/v) followed by acetone, and finely ground using a mortar and pestle, followed by
130 grinding between two polished glass plates (12). The resulting fine powders were

131 rehydrated in endotoxin-free PBS containing 30 mM EDTA (1 ml for every 2 mg dry
132 mass) to extract the calcium inositol hexakisphosphate deposits, thus leaving the mucin
133 meshwork as single major structural component (3). The material was then extensively
134 washed into endotoxin-free PBS. To obtain a fine particulate preparation (pLL), the
135 suspension was filtered through 85- and 23-µm gauze (12). To obtain the soluble
136 preparation (sLL), the suspension was subjected to sonication followed by centrifugation
137 for 1 h at 100,000 g at 4°C. To obtain sLL in which the terminal monosaccharide residues
138 were oxidized, prior to the solubilization step, the material was treated with sodium
139 periodate followed by sodium borohydride (or with sodium borohydride only as mock
140 treatment) (12). For obtaining biotin-tagged sLL, prior to the solubilization step, the
141 material in PBS was incubated overnight with N-hydroxysuccinimido-biotin (NHS-
142 biotin; 10 ng per mg of LL dry mass). Sodium periodate, sodium borohydride and/or
143 NHS-biotin were removed by extensive washing of the particles into endotoxin-free PBS.
144 Destruction of terminal monosaccharides by periodate was verified in terms of abrogation
145 of the binding biotinylated PNA (24), revealed with the help of streptavidin-perodixase,
146 in a dot-blot format. Biotin incorporation by the sLL was checked using streptavidin-
147 peroxidase also in dot-blot format. The dry mass content of LL mucin preparations was
148 estimated as in (12). LL mucin preparations were stored at 4°C in PBS with penicillin-
149 streptomycin during no more than 6 months (pLL) or 12 months (sLL).
150
151 *Clec4f$^{-/-}$ mouse line generation*
152
153 Although Clec4f$^{-/-}$ mice had been previously generated by one of the authors' group
154 (16), the cost of importing the mice from Taiwan to Uruguay and re-deriving them was
155 high enough that made *de novo* generation of a Clec4f$^{-/-}$ line by CRISPR-Cas9

156 technology economically convenient. All animal procedures were performed at the
157 Specific Pathogen Free animal facility of the Laboratory Animal Biotechnology Unit of
158 Institut Pasteur de Montevideo. Experimental protocols were approved by the
159 Institutional Animal Ethics Committee (protocol number 007-18), in agreement with
160 National law 18.611 and international animal care guidelines (Guide for the Care and
161 Use of Laboratory Animals) (25) regarding laboratory animal's protocols. Mice were
162 housed in individually ventilated cages (Tecniplast, Milan, Italy) containing chip
163 bedding (Toplit 6, SAFE, Augy, France), in a controlled environment at 20 ± 1ºC with a
164 relative humidity of 40-60%, in a 14/10 h light-dark cycle. Autoclaved food (Labdiet
165 5K67, PMI Nutrition, IN, US) and autoclaved filtered water were administered *ad*
166 *libitum*. Cytoplasmic microinjection was performed in C57BL/6J zygotes using a mix of
167 25 ng/µl Cas9 mRNA (Invitrogen, Carlsbad, CA, US), 15 ng/µl of each sgRNA (2
168 guides were used) (Synthego, Menlo Park, CA, US), diluted in standard microinjection
169 buffer (5 mM Tris-HCl, pH 7.4, 0.1 mM EDTA). Viable embryos were cultured
170 overnight in M16 (Sigma, St Louis, MO, US) microdrops under embryo tested mineral
171 oil (Sigma), with 5% CO_2 in air at 37 ºC. The next day, 2-cell embryos were transferred
172 into the oviduct of B6D2F1 0.5 days postcoitum pseudopregnant females (20
173 embryos/female in average). Standard surgical procedures established in our animal
174 facility were followed (26). For surgery, recipient females were anesthetized with a
175 mixture of ketamine (110 mg/kg, Ketonal50, Richmond Veterinaria S.A., Buenos Aires,
176 Argentina) and xylazine (13 mg/kg, Seton 2%; Calier, Montevideo, Uruguay).
177 Tolfenamic acid was administered subcutaneously (1 mg/kg, Tolfedine, Vetoquinol,
178 Madrid, Spain) in order to provide analgesia and anti-inflammatory effects (27).
179 Pregnancy diagnosis was determined by visual inspection by an experienced animal
180 caretaker two weeks after embryo transfer, and litter size was recorded on day 7 after

181 birth. Pups were tail-biopsied and genotyped 21 days after birth, and mutant animals
182 were maintained as founders. Gene editing efficiency was 53.8% (7 KO/13 born pups).
183 Genetic modification was confirmed by Sanger sequencing. The Clec4f$^{-/-}$ line was
184 established after producing F1, F2, and finally homozygous F3 animals that were used
185 for experiments. Primers used for amplification of the genomic locus were 5'-
186 TCTTTATGATCGCACCCACA-3', 5'-TCCATTCTCGAGAGCCATCT-3'. F1 and F2
187 heterozygous mice were selected using a heteroduplex mobility assay on a 10%
188 polyacrylamide gel. In F2, WT animals were differentiated from homozygous KO
189 animals by Sanger sequencing.
190
191 *Mouse experiments*
192
193 WT BALB/c mice were obtained from DILAVE (MGAP, Uruguay) and kept at the
194 Instituto de Higiene animal house. Female WT (C57BL/6J) or Clec4f$^{-/-}$ mice were bred
195 at the Institut Pasteur de Montevideo, co-housed (so as to equilibrate their microbiota) at
196 the Instituto de Higiene starting at 5 weeks of age for at least 3 weeks, and used between
197 8 and 14 weeks of age. sLL (100 or 200 μg dry mass per mouse as indicated in each case,
198 dissolved in 100 μl of PBS) or vehicle only was injected into the tail vein. pLL (450 μg
199 dry mass per mouse, suspended in 200 μl of PBS) or vehicle only, were injected i.p. Mice
200 were infected by i.p. injection of 2000 (BALB/c) or 2500 (C57BL/6) protoscoleces
201 (viability ≥ 95%) suspended in 200 μl of PBS; control mice were injected with vehicle
202 only. Mice were euthanized using isoflurane. The procedures used were approved by the
203 Comisión Honoraria de Experimentación Animal (CHEA, Universidad de la República,
204 Uruguay: protocols 101900-001017-16, 101900-000994-16, 101900-000649-17,
205 101900-000441-16).

206

207 *Preparation of liver non-parenchymal fraction for flow cytometry*

208

209 Following perfusion through the inferior vena cava with 10 mL of PBS, livers were placed
210 in RPMI and finely chopped using a razor blade for approximately 2 min. The tissue was
211 then digested in 5 ml per g of enzyme mix (RPMI containing 0.4 U/ml Liberase [Sigma]
212 and 80 U/ml DNase [Sigma]), for 25 min at 37◦C, in an orbital shaker at 250 rpm with
213 additional manual shaking every 5 min. Digests were poured through a 100 µm strainer
214 and centrifuged at 300 g for 5 min; the cell pellets were re-suspended in 25 ml of RPMI
215 and again centrifuged at 300 g. The pellets were suspended in 2 ml of RBC lysis buffer
216 (Sigma), and after 2 min, 2 ml of FACS buffer (PBS supplemented with 0.5% BSA and
217 2 mM EDTA) was added. After another centrifugation step (300 g, 5 min), cells were re-
218 suspended in 3 ml of FACS buffer, passed through a 40 µm strainer, and counted using
219 the Nexcelom Cellometer K2 with the AOPI stain for cell viability. Cells and buffer used
220 with the cells were kept at 4ºC, except for the digestion step.

221

222 *Flow cytometry*

223

224 Five hundred thousand live cells where incubated with the viability probe for 10 min at
225 room temperature, then with 0.025 µg of anti-CD16/32 (Biolegend) in 10% v/v normal
226 rat serum (Unidad de Reactivos y Biomodelos de Experimentación, Facultad de
227 Medicina, Universidad de la República). Cells were then surface-stained, fixed in 1% w/v
228 PFA for 20 min at 4°C, washed, and permeabilized overnight with permeabilisation
229 buffer (Thermo) for intracellular staining. The details of the viability probes, antibodies
230 and lectin probes are given in Supplementary Table 1. Finally, cells were washed, spun

231 at 350 g for 5 min and re-suspended in FACs buffer. The data were acquired in a FACS
232 Canto II Cytometer (BD), at the Instituto de Higiene, Universidad de la República, and
233 then analysed using the FlowJo software package. The relative contribution of each liver
234 non-parenchymal cell type under study to the uptake of LL materials was estimated by
235 multiplying the frequency of cells positive for the LL probe and belonging to the
236 particular cell type (within all live single cells) by their arithmetic mean fluorescence
237 intensity for the probe and then dividing this figure over the summation of the analogous
238 products for the 3 cell types analysed.
239
240 *Histology*
241
242 Tissue pieces (approximately 0.5 mm^3) were fixed in buffered formalin. Liver samples
243 corresponded to animals subjected to liver perfusion with PBS (as the materials were also
244 analyzed by flow cytometry). Paraffin-embedded tissue sections (2 µm) were probed with
245 biotinylated monoclonal antibody E492 (3 µg/mL; steamer pH 6.1) or biotinylated PNA
246 (Vector Laboratories, Newark, California, United States, B-1075; dilution 1:100; steamer
247 pH 9.0) using the avidin-biotin-complex method (28), and counterstained using
248 haemalum.
249
250 *ELISA*
251
252 ELISA wells were coated with sLL at 10 µg/mL (total dry mass) in Tris-buffered saline
253 (TBS) overnight at 4 ºC, and blocked using TBS containing 0.05% w/v Tween 20, 1%
254 w/v bovine serum albumin and 0.5% v/v Carbo-Free™ blocking solution (Vector
255 Laboratories). Wells were then probed with biotinylated E492 antibody (29), biotinylated

256 peanut agglutinin (PNA; Vector laboratories) or recombinant soluble Clec4F (expressed
257 as a fusion with the F_c fragment of human IgG_1 (30)). The biotinylated PNA or E492
258 antibody were detected using streptavidin coupled to peroxidase (ThermoFisher
259 Scientific) and the recombinant Clec4F was detected using a goat anti-human IgG
260 coupled to peroxidase (AbCam, Cambridge, UK). For competition ELISA, recombinant
261 Clec4F at 80 ng/mL was mixed with variable concentrations of either (biotinylated) PNA
262 or E492 antibody as competitors, and bound Clec4F detected as previously described.
263
264 *Particle immunofluorescence*
265
266 pLL particles were incubated with biotinylated E492 antibody (0.6 µg/mL), biotinylated
267 PNA (1:1500) or recombinant soluble Clec4F (7.5 µg/mL), followed by streptavidin-
268 Cyanine-3 (1:500; Amersham Bioscience) or by goat anti-human IgG coupled to FITC
269 (1:100, Sigma), as appropriate. Control stains were included using human IgG_1 instead
270 of recombinant Clec4F as well omitting the primary staining reagents.
271
272 *Statistical analyses*
273
274 As the underlying data do not satisfy the criteria for parametric statistics, rank-based
275 nonparametric statistical methods, were used throughout. When the numbers of mice in
276 each treatment-repeat experiment combination were equal, the Mack-Skillings exact test
277 for a two-way layout was used (31). When the data did not fulfil the above condition, data
278 from the different repeat experiments were pooled and the modified Wilcoxon-Mann-
279 Whitney test (only two experimental groups) (53) or the Kruskal-Wallis test (more than
280 two experimental groups) were used. When the Mack-Skillings or the Kruskal-Wallis

281 tests resulted in a statistic with a p-value less than 0.05, the test was followed by the post-
282 hoc multiple comparison test described by Conover (55) and the Benjamini-Hochberg
283 correction for controlling the false discovery rate (56). Throughout the paper, the symbols
284 *, ** and *** represent p-values less than 0.05, 0.01 and 0.001 respectively.
285
286 **Results**
287
288 *Soluble LL mucins are taken up by Kupffer cells* in vivo *in a manner dependent on the*
289 *mucin glycans*
290
291 We first sought to determine whether KC take up soluble LL mucins (sLL) *in vivo* and
292 whether this is dependent on the mucin glycans. We thus treated the LL mucins either
293 with sodium periodate to oxidize the glycans or applied a mock treatment, tagged both
294 preparations with equivalent amounts of biotin (Fig. S1), and injected both preparations
295 i.v. in mice. Twenty minutes later, we quantitated the biotin tag in permeabilized non-
296 parenchymal liver cells using streptavidin conjugated to PE and flow cytometry. KC were
297 identified using our previously validated gating strategy (Fig. S2) (32). A significant
298 signal was detected in KC, and the signal was markedly higher for mock-treated than for
299 periodate-treated sLL (Fig. 1). No significant biotin signal was detected in either LSECs
300 or in non-KC $CD11b^+$ cells, a broad definition that encompasses any mononuclear
301 phagocytes other than KC present in the liver (Fig. 1 a, b, and S2).
302
303 *The plant lectin PNA and the E492 monoclonal antibody allow detection of laminated*
304 *layer mucins captured by liver cells* in vivo.
305

306 Except in experiments using periodate-treated LL materials, the detection of LL materials
307 by appropriate carbohydrate-binding probes was preferable to prior labelling with biotin.
308 Among other advantages, such probes would allow the detection of endogenous LL
309 mucins in infected animals. One candidate probe was the plant lectin PNA, which binds
310 Galβ1-3-GalNAcα1-peptide, i.e. the non-decorated mucin O-glycan core 1 or T-antigen
311 (33). This motif is highly represented in the *E. granulosus* LL, and accordingly, PNA
312 binds the LL mucins in histological sections, particle lectin fluorescence, and Western
313 blotting (12, 24). The second candidate probe was the monoclonal antibody E492, raised
314 against *E. granulosus* protoscoleces (34). This antibody binds to LL mucins from *E.*
315 *multilocularis* (35) and to synthetic glycans that include the P_1 blood antigen motif
316 (Galα1-4Galβ1-4GlcNAc), highly represented among *E. granulosus* LL mucin glycans
317 (7, 8). A third potential probe was recombinant Clec4F (13). We verified that these
318 potential probes indeed bind to sLL coated on ELISA plates as well as to LL particles in
319 suspension (Fig. 2 a, b).
320
321 We took advantage of the defined specificities of PNA and the E492 antibody to gain
322 insight into the carbohydrate motifs bound by Clec4F in the LL mucins. The binding of
323 recombinant Clec4F to the solubilized and plate-bound LL mucins was not competed by
324 PNA, but it was strongly competed by the E492 antibody (Fig. 2 c). Therefore, most of
325 the binding of Clec4F to the native LL mucins appears to rely on recognition of the P_1
326 motif, whereas recognition of the T-antigen is not significant. This in turn suggests that
327 in the LL mucins the T-antigen may not be exposed and/or be spaced inadequately for
328 Clec4F binding, as recombinant Clec4F does bind the T-antigen in glycan arrays (15–17).
329

330 *In vivo* probes should show minimal reactivity with host tissues; for our purposes, lack of
331 reactivity with the populations of mouse non-parenchymal liver cells under study was the
332 most important consideration. Neither PNA nor the E492 antibody showed significant
333 binding in flow cytometry to KC or LSEC from control mice (Fig. S3). PNA bound to a
334 very minor fraction of non-KC $CD11b^+$ cells, whereas the antibody did not bind. PNA,
335 but not the E492 antibody, bound to a major sub-population of $CD45^+$ $CD11b^-$ $F4/80^-$
336 cells, which were not of particular interest in our study. Recombinant Clec4F bound to
337 cells in all 4 cell gates defined, most strongly to LSEC and KC (Fig. S3). This probably
338 reflects the fairly broad specificity of Clec4F for glycans terminated in Gal/GalNAc (15–
339 17), and ruled out this lectin as a probe for our purposes.
340
341 Finally, to determine whether uptake of sLL could be measured *in vivo* using PNA or the
342 E492 antibody, we injected wild-type (WT) C57BL/6J mice i.v. with sLL and
343 subsequently stained isolated hepatic non-parenchymal cells intracellularly with either
344 probe. As expected, no staining was observed in cells from mice injected with PBS only,
345 whereas KC, and to a small extent also LSEC, from mice given sLL stained intracellularly
346 with either PNA or E492 antibody (Fig. 2 d). Omitting the cell permeabilization step
347 caused the PNA signal in KC and LSEC of sLL-injected mice to be reduced to negligible
348 levels (data not shown), ruling out the remote possibility that injection of sLL induces the
349 expression of ligands for the probe in the glycocalix of the cells under study. Both PNA
350 and the E492 antibody appeared to allow more sensitive detection than prior labelling
351 with biotin (Fig. 1), so that captured sLL was detected in almost all KC and also in some
352 LSEC.
353

354 In summary both PNA and the E492 antibody are useful probes for LL mucins captured
355 by mouse non-parenchymal liver cells.
356
357 *Soluble LL mucins are taken up by Kupffer cells* in vivo *in a manner dependent on Clec4F*
358
359 We first used CRISPR/Cas9 to generate a new Clec4f $^{-/-}$ line on the C57BL/6J
360 background. These Clec4f $^{-/-}$ mice have 8-bp deletion expected to result in a polypeptide
361 that is truncated near the N-terminus (Fig. 3, a, b), and effectively lack Clec4F protein
362 expression by flow cytometry (Fig. 3 c). Hence, our line appears similar to Clec4f gene-
363 deficient mice that have already been described (16, 19).
364
365 We next compared WT and Clec4f$^{-/-}$ mice in terms of the *in vivo* uptake of sLL by liver
366 non-parenchymal cells. For this purpose, we injected untagged sLL, either untreated or
367 subjected to the mock treatment used in the previous experiments that involved periodate
368 oxidation. Uptake of sLL by KC was strongly dependent on Clec4F (Fig. 4 a - c),
369 particularly when assessed in terms of mean fluorescence intensity. The low-level uptake
370 by LSEC observed was as expected independent of Clec4F; in fact, for untreated sLL,
371 uptake by LSEC was slightly enhanced in the absence of Clec4F, possibly as a result of
372 the decreased capture by KC. No uptake by non-KC CD11b^{+} cells was detected (Fig. 4 a,
373 b and Fig. S4). Through a calculation that takes into account the numbers of each cell
374 type capturing sLL and the intensity of the signal indicating intracellular sLL, KC were
375 estimated to be responsible for the overwhelming majority of sLL uptake by non-
376 parenchymal liver cells in WT mice (Fig. 4 d). However, in the absence of Clec4F, LSEC
377 played a significantly, if slightly, more important part in the uptake of sLL than in the
378 presence of the receptor. Differences in the uptake of untreated *vs* mock-treated material

379 were not observed, except in the low-level uptake by LSEC in Clec4f$^{-/-}$ mice (Fig. 4 a).
380 For consistency with the results shown in Figure 1, we chose to use mock-treated material
381 in the following experiments.
382
383 It can be expected that in the absence of Clec4F, other mechanisms of cellular uptake of
384 sLL may become apparent, e.g. macropinocytosis or uptake dependent on natural
385 antibodies or complement (6). Such Clec4F-independent uptake of sLL was hinted by the
386 previous observations in relation to LSEC, as well as by the 25 – 60 % KC in Clec4f$^{-/-}$
387 mice positive for PNA at low levels (Fig. 4 a - c). As the Clec4F-independent mechanisms
388 might become dominant at longer analysis times, we carried out a similar experiment with
389 a 22 h analysis time. Uptake of sLL was still dominated by KC among the cell types
390 studied, and this uptake was again strongly dependent on Clec4F (Fig. 5 a –d). In the
391 absence of Clec4F, LSEC made a significantly larger contribution to sLL uptake than in
392 the presence of the receptor, but this contribution was still minimal (Fig. 5 d). Non-KC
393 CD11b^{+} cells did not take up material detectably (Fig. 5 a – d and S4). Cell surface
394 expression of Clec4F in KC was not altered by sLL injection (Fig. S5).
395
396 In summary, soluble circulating LL mucins in naïve mice are taken up mainly by KC
397 among liver non-parenchymal cells and mostly in Clec4F-dependent fashion.
398
399 *LL mucins injected in particulate form are taken up* by *Kupffer cells* in vivo *in Clec4F-*
400 *dependent manner*
401
402 Although the release of soluble mucins from the LL during cystic echinococcosis is a
403 possibility (6), only particles have been documented to be shed from the LL in human

404 infections (6, 10). It is not known if these particles circulate systemically and/or give rise
405 to soluble materials that circulate. It was therefore important to determine whether Clec4F
406 participates in the uptake by KC of LL mucins released in a particulate presentation into
407 the internal milieu and at an anatomical site distant from the liver. We thus injected i.p.
408 particulate LL mucins (pLL) (12), and analysed the liver non-parenchymal fraction 22 h
409 later. LL material was indeed detected by flow cytometry in KC (Fig. 6 a – c and S6 a -
410 c). Uptake by KC was dependent on Clec4F, although there was a considerable degree of
411 Clec4F-independent uptake as well. In addition to low-level uptake by LSEC, in this
412 experimental system, non-KC $CD11b^+$ cells were observed to take up the LL material.
413 Although non-KC $CD11b^+$ cells may include recruited monocytes/macrophages, the
414 frequency of this population (within all non-parenchymal cells) did not increase as a result
415 of pLL injection (Fig. S7). As expected, uptake by LSEC and by non-KC $CD11b^+$ cells
416 was independent of Clec4F and in fact tended to be enhanced in the absence of the
417 receptor (Fig. 6 a – c and S6 a - c). Indeed, whereas in WT mice the overwhelming
418 majority of the LL material uptake by liver non-parenchymal cells was carried out by KC,
419 in $Clec4f^{-/-}$ mice the two non-KC cell types studied taken together played a significantly
420 larger role than in WT mice (Fig. 6 d and S6 d). The cell surface expression of Clec4F in
421 KC was not altered by injection of pLL (Fig. S8).
422
423 The mostly Clec4F-dependent uptake of the LL material was confirmed by histology,
424 using the E492 antibody as a probe. Strong staining was observed in KC-like cells of WT
425 animals, whereas only minimal staining was observed in the KC-like cells of $Clec4f^{-/-}$
426 animals (Fig. 6 e). Animals injected with pLL also showed weak staining in hepatocytes
427 (a cell type not analysed by flow cytometry), and this was independent of Clec4F. As
428 hepatocytes are unlikely to phagocytose large particles, this observation suggests the

429 particles injected release small particles and/or soluble mucin materials *in vivo* that
430 preferentially circulate systemically.
431
432 In summary, LL mucins present within tissues in particulate form can generate materials
433 (particulate and/or soluble) that circulate systemically and that are captured by KC via
434 Clec4F.
435
436 *In experimental* E. granulosus *infection, LL mucins circulate and are captured selectively*
437 *by Kupffer cells, with the participation of Clec4F*
438
439 We next wished to determine if Clec4F was relevant in the infection setting. The most
440 widely used experimental infection model for *E. granulosus* uses intraperitoneal injection
441 with protoscoleces, parasite stages that usually develop into adult worms but are capable
442 of reverse development into hydatids (1, 36). In this model, hydatids develop free or
443 within host collagen capsules in the peritoneal cavity (37). KC uptake of LL materials in
444 this model would require that such materials reach systemic circulation, a possibility for
445 which there was no evidence, in experimental or natural infections. We first analysed
446 infected mice of the BALB/c strain, in which experimental infection reaches higher
447 parasite burdens than in the C57BL/6 strain (38). Indeed, the BALB/c mice analysed had
448 a median of 25 mL of total parasite volume (Fig. S9 a), an extremely high parasite burden.
449 In these mice, using the E492 antibody as probe, we detected LL materials by histology
450 in peritoneal cavity cells (i.e. the site of infection) and the liver, but not in kidneys,
451 intestine or lungs (Fig. 7 a). In addition, in some of the infected mice, occasional positive
452 cells were observed in the spleen, and less frequently in the mesenteric lymph nodes (Fig.
453 7 a). The use of PNA as probe yielded similar results, but it was complicated by the

454 expected signal in the lymphoid organs (39) unrelated to LL material, i.e. detectable in
455 non-infected mice (data not shown).
456
457 The above results show that in infected animals LL mucins circulate systemically and
458 become selectively concentrated in the liver. Within the liver, the signal for LL mucins
459 was specifically concentrated in KC-like cells (Fig. 7 a). The LL signal in KC-like cells
460 was observed in 12 out of 15 infected mice analysed. Contrary to previous experiments
461 injecting pLL, no signal was detected in hepatocytes. This may be related to lower loads
462 of LL material, as suggested by the lower intensity in the staining in KC in the infection
463 setting in comparison to the pLL injection experiments (compare Fig. 6 e and 7 a).
464
465 The selective LL material uptake by KC among the liver non-parenchymal cells was
466 confirmed by flow cytometry (Fig. 7 b – d and S10). Although the data did not reach
467 statistical significance, a sub-population of non-KC CD11b^{+} cells appeared to take up LL
468 materials (Fig. 7 b – d). Also, the frequency of non-KC CD11b^{+} cells within all liver non
469 parenchymal cells was significantly increased by infection, suggesting cell recruitment
470 (Fig. S11 a). The cell surface expression of Clec4F in KC was not altered by infection
471 (Fig. S12 a).
472
473 We next analysed infected C57BL/6 WT and Clec4f$^{-/-}$ mice. In these mice, the parasite
474 burdens were low: the median burden in the WT C57BL/6 mice was 0.5 mL (this figure
475 corresponds to the two infection experiments fully analysed, as an additional experiment
476 with very low parasite burdens was excluded from analysis). Although the median
477 parasite burden was 3-fold lower in Clec4f$^{-/-}$ mice than in WT mice, the trend did not
478 reach statistical significance (Fig. S8 b). By flow cytometry, uptake of LL material by

479 KC was detected, in WT but not in Clec4F$^{-/-}$ mice (Fig. 7 e - g). No significant uptake
480 was detected in LSECs (Fig. 7 e, f and S10 b). In non-KC CD11b^{+} cells, there was a trend
481 towards low-level, Clec4F-independent uptake (Fig. 7 e - g), which did not reach
482 significance. The frequency of non-KC CD11b^{+} cells was not significantly altered by
483 infection (Fig. S 11 b). Again, Clec4F surface expression in the KC of WT mice was not
484 altered by infection (Fig. S12 b).
485
486 **Discussion**
487
488 In this article we show that native LL materials shed from *E. granulosus sensu lato*
489 hydatids are taken up selectively by KC, in a fashion mostly dependent on Clec4F. It is
490 thought that pathogens capable of immune evasion engage innate receptors that normally
491 bind altered self, as opposed to receptors specialized in detecting pathogens and triggering
492 inflammatory responses (40). *E. granulosus* is well adapted for immune evasion (2), and
493 the fact that its most abundant surface molecules engage a receptor involved in the
494 clearing of aged host platelets (19, 20) seems to be in line with the above principle.
495
496 KC are specialized in removing unwanted materials from the blood. Our results imply
497 that the LL mucins (which even after their artificial solubilisation behave as having very
498 high molecular sizes (24)) have the capacity to circulate systemically, thus reaching KC
499 from a distant anatomical site. This applies to exogenous LL mucins initially present in
500 the peritoneal cavity in particulate format, which must therefore either circulate as
501 particles and/or partly solubilize *in vivo*. It also applies to the LL materials released by
502 live parasites growing in the peritoneal cavity.
503

504 In addition to KC, both LSEC and certain non-KC CD11b$^+$ cells were observed to take
505 up LL materials. This was in both cases independent of Clec4F, and in some experimental
506 settings it was enhanced in the absence of Clec4F (Fig. 4 d, 6 d and S6 d). Uptake of
507 materials by non-KC CD11b$^+$ cells was apparent after injection of LL mucins in
508 particulate presentation (pLL; Fig. 6 a – d and S6) but not in a soluble presentation (sLL;
509 Fig. 1, 4 and 5). This contrast suggests that the species released *in vivo* from the large LL
510 particles and capable of circulating are (or at least include) small particles, as opposed to
511 fully soluble mucins like those making up sLL. The fact that uptake by the non-KC
512 CD11b$^+$ population was clear after injection of a high-dose bolus of pLL whereas it was
513 merely hinted in experimental infection (Fig. 7 b - g) is most probably explained by this
514 uptake mechanism becoming relevant only when the uptake capacity of KC is
515 overwhelmed. It is unlikely that the non-KC CD11b$^+$ cell population taking up LL
516 materials derives from peritoneal cavity macrophages, as it is composed of F4/80$^-$ cells
517 (Fig. 6 c and S6 c), whereas most resident peritoneal macrophages as well as peritoneal
518 macrophages reported to enter the liver upon injury to this organ are F4/80^{hi} (41). We
519 instead favour the possibility that the population being discussed corresponds to
520 monocytic cells present in the liver or recruited in response to LL particles physically
521 trapped in the liver sinusoids.
522
523 Hepatocytes could be an additional target cell for LL materials in the liver, as suggested
524 by the weak but significant staining observed in this cell type after pLL injection (Fig. 6
525 e). The obvious candidate receptor to mediate this apparent uptake is the ASGR (42).
526 Ligand uptake by hepatocytes via the ASGR is reported to have an upper size limit of 70
527 nm (43). Thus the signal in hepatocytes observed in our experiments with pLL (which
528 has particle sizes in the micrometer range (12)) may correspond to uptake of soluble

529 mucins released from the particles *in vivo*. In the same experiments as well as in the
530 infection experiments (Fig. 7), the preferential uptake by KC in relation to hepatocytes
531 surely reflects the differential capacity of KC to phagocytose particles (even if
532 additionally, Clec4F may bind LL mucins better than the ASGR, as suggested by *in vitro*
533 evidence (13)). Our results do not allow to weigh the importance of hepatocytes in the
534 capture of fully soluble injected LL materials (sLL).
535
536 Part of the uptake of LL materials by KC was observed to be Clec4F-independent (Fig. 5
537 a, 6 a, b, and 7 e). Clec4F-independent uptake by KC, as well as by non-KC $CD11b^+$ cells
538 and LSEC as previously mentioned, may be mediated by natural anti-carbohydrate
539 antibodies that bind the LL mucins, either directly or via complement activation (44). In
540 the context of chronic experimental infection, the possibilities for Clec4F-independent
541 uptake are even broader than after LL mucin injection. In the first place, the mucins will
542 be opsonized by specific (homologous) antibodies (6, 44). In second place, contrary to
543 the artificially prepared (soluble and insoluble) mucin preparations, LL materials shed
544 from live parasites must contain the major non-mucin structural component of the LL,
545 i.e. calcium inositol hexakisphosphate (calcium InsP_6) (45–47). Calcium InsP_6 binds host
546 C1q and initiates limited activation of complement (44, 48). In fact, the observed uptake
547 of LL materials by phagocytes at the experimental infection site (Fig. 7 a) must also be
548 Clec4F-independent, as peritoneal macrophages are not expected to express Clec4F (16).
549 Given the ample possibilities of Clec4F-independent capture, it is noteworthy the Clec4F
550 nonetheless has a clearly detectable role in LL material uptake (by KC), especially in the
551 infection context.
552

553 As mentioned, in human infections affecting solid organs, LL debris accumulate in the
554 parasite's vicinity (10). Our results show the presence of LL materials at the experimental
555 infection site but also as mentioned the capture of these materials by the liver (Fig. 7 a).
556 This implies that the accumulation of LL debris in the parasite's vicinity is moderated by
557 the circulation and capture by the liver of materials derived from this debris. This is
558 important because, although moderate amounts of LL particles probably have immune
559 modulatory effects that favour the parasite, large amounts of LL particles accumulating
560 at the infection site would probably foster inflammation (11, 12, 49, 50). Inflammation
561 might also be brought about the LL materials remaining in circulation and possibly being
562 deposited in the glomeruli or other sites. Indeed, if as we speculated above, monocytes
563 are recruited to the liver in response to trapped LL particles, then Clec4F-dependent KC
564 capture may be important to avoid liver inflammation. This aspect may not have been
565 fully captured in our flow cytometry and histology experiments because of liver perfusion
566 prior to analysis.
567
568 The events downstream of LL material capture by KC are certainly worth studying. KC
569 can present antigens to T cells present in the vascular space, and this normally leads to
570 tolerogenic responses that can have a systemic impact (22, 51, 52). The analysis of
571 immune responses in WT and Clec4f$^{-/-}$ mice infected with *E. granulosus* will be the
572 subject of a future communication.
573
574 Ancestrally, the larval stages of the parasites belonging to the taeniid family (including
575 those of the genus *Echinococcus*) probably infected the liver of rodent hosts (5, 53). In
576 this context, the interaction of materials shed by the parasites with a receptor (Clec4F)
577 specifically expressed by phagocytic cells present in the same organ (KC) may have been

578 evolutionarily advantageous. This may have been so because LL material uptake by KC
579 would have avoided particle build-up and consequent inflammation in the liver sinusoids
580 and/or other sites, and/or because KC are poised for tolerogenic antigen presentation. The
581 extant species *E. multilocularis* dwells almost exclusively in the liver of rodents (besides
582 accidentally infecting humans). The LL of this species also interacts with Clec4F, as
583 suggested by experiments using recombinant Clec4F (13) and by the presence in this
584 species' LL of the blood antigen P_1 motif (54). Thus, host Clec4F is likely an important
585 player in *E. multilocularis* infection.
586
587 The natural hosts of larval *E. granulosus* are mostly ungulates, including sheep, cattle,
588 pigs, goats, camels and horses. Like in rodents, in ungulates Clec4F also appears to be
589 expressed in the liver (15). Therefore, the uptake of LL materials by KC via Clec4F
590 probably takes place also in the ungulate natural hosts. However, in ungulates Clec4F
591 appears to be additionally expressed in secondary lymphoid organs (15), opening the
592 possibility that non-KC, anatomically more widely distributed, phagocytes may act as
593 additional sinks for LL materials.
594
595 As mentioned, humans do not express Clec4F with a functional lectin domain (15).
596 Humans are normally a dead-end for this parasite's life-cycle, meaning that human
597 *Echinococcus* infection has not been shaped through evolution. Although *E.*
598 *multilocularis* infection in humans is usually accompanied by strong local inflammation
599 (and tissue destruction), this is not usually the case with *E. granulosus* (9, 55). It is a
600 possibility that for *E. granulosus*, which grows more slowly than *E. multilocularis*,
601 Clec4F-independent clearance mechanisms are in most infection settings sufficient to
602 avoid excessive build-up of LL debris. It is conceivable that such Clec4F-independent

603 mechanisms in humans include uptake via lectins expressed in KC with specificities
604 related to Clec4F. As mentioned, the uptake of de-sialylated platelets by mouse KC
605 requires Clec4F as well as MGLs or ASGR (19, 20). It seems likely that a mechanism for
606 de-sialylated platelet uptake by KC based on a set of collaborating lectins exists
607 throughout mammals, even if in humans such a system does not include Clec4F. Our
608 previous screening using recombinant receptors yielded inconclusive results with respect
609 to the capacity of human MGL and ASGR to interact with the LL mucins (13). When
610 probing synthetic sugars, human ASGR and MGL appeared to bind less well than Clec4F
611 to the P_1 motif (after normalizing by binding to a known target of all 3 receptors) (13).
612 However, given the sheer abundance and significant breadth of Gal-based motifs in the
613 LL, it would not be surprising if ASGR and/or MGL were able to internalize LL materials
614 in the absence of Clec4F. It is important to determine if KC in liver samples from humans
615 infected with *E. granulosus*, as well as with *E. multilocularis*, stain for LL materials.
616
617 **Statement of Ethics**
618 Mouse studies followed the ARRIVE guidelines. Experimental protocols were
619 individually reviewed and approved by the Institutional Animal Ethics Committees of the
620 Institut Pasteur Montevideo or the Universidad de la República, Uruguay, as detailed in
621 the Materials and Methods section.
622
623 **Conflict of Interest Statement**
624 The authors declare no conflict of interest.
625
626
627

Funding sources

This work was funded by Agencia Nacional de Investigación e Innovación (ANII; Government of Uruguay) grant FCE 136130 (to AD), by a Travel Grant (to SJJ) from the Science and Innovation Fund of the Foreign and Commonwealth Office (UK Government), and by PEDECIBA (Government of Uruguay). AB and CM were supported by PhD scholarships from Comisión Académica de Posgrado (Universidad de la República, Uruguay) and ANII respectively.

Author contributions

AB: conceptualization, investigation. CM, LS, JN, MS: investigation. GS, MNM, APM, MC: methodology. TLH, SLH, GME: resources. CG: formal analysis (statistics). TFEB, CC: conceptualization, supervision. SJJ: conceptualization, funding acquisition, supervision, writing – review & editing. AD: conceptualization, funding acquisition, project administration, supervision, writing – original draft preparation.

646 **References**

647

648 1. Thompson RCA. 2017. Biology and Systematics of Echinococcus. Adv Parasitol
649 95:65–109.

650 2. Díaz Á. 2017. Immunology of cystic echinococcosis (hydatid disease). British
651 Medical Bulletin 124:121–133.

652 3. Díaz A, Casaravilla C, Irigoín F, Lin G, Previato JO, Ferreira F. 2011.
653 Understanding the laminated layer of larval Echinococcus I: structure. Trends in
654 Parasitology 27:204–213.

655 4. Díaz A, Casaravilla C, Allen JE, Sim RB, Ferreira AM. 2011. Understanding the
656 laminated layer of larval Echinococcus II: immunology. Trends in Parasitology
657 27:264–273.

658 5. Díaz Á, Fernández C, Pittini Á, Seoane PI, Allen JE, Casaravilla C. 2015. The
659 laminated layer: Recent advances and insights into Echinococcus biology and
660 evolution. Experimental Parasitology 158:23–30.

661 6. Díaz A, Barrios AA, Grezzi L, Mouhape C, Jenkins SJ, Allen JE, Casaravilla C.
662 2022. Immunology of a unique biological structure: the Echinococcus laminated
663 layer. Protein & Cell https://doi.org/10.1093/procel/pwac023.

664 7. Lin G, Todeschini AR, Koizumi A, Neves JL, González H, Dematteis S, Hada N,
665 Previato JO, Ferreira F, Mendonça-Previato L, Díaz A. 2013. Further structural
666 characterization of the Echinococcus granulosus laminated layer carbohydrates:
667 The blood-antigen P1-motif gives rise to branches at different points of the O-
668 glycan chains. Glycobiology 23:438–452.

669 8. Díaz A, Fontana EC, Todeschini AR, Soulé S, González H, Casaravilla C, Portela
670 M, Mohana-Borges R, Mendonça-Previato L, Previato JO, Ferreira F. 2009. The
671 Major Surface Carbohydrates of the *Echinococcus granulosus* Cyst: Mucin-Type
672 *O* -Glycans Decorated by Novel Galactose-Based Structures. Biochemistry
673 48:11678–11691.

674 9. Díaz Á, Sagasti C, Casaravilla C. 2018. Granulomatous responses in larval taeniid
675 infections. Parasite Immunol 40:e12523.

676 10. Grimm J, Nell J, Hillenbrand A, Henne-Bruns D, Schmidberger J, Kratzer W,
677 Gruener B, Graeter T, Reinehr M, Weber A, Deplazes P, Möller P, Beck A, Barth
678 TFE. 2020. Immunohistological detection of small particles of Echinococcus
679 multilocularis and Echinococcus granulosus in lymph nodes is associated with
680 enlarged lymph nodes in alveolar and cystic echinococcosis. PLoS Negl Trop Dis
681 14:e0008921.

682 11. Pittini Á, Martínez-Acosta YE, Casaravilla C, Seoane PI, Rückerl D, Quijano C,
683 Allen JE, Díaz Á. 2019. Particles from the Echinococcus granulosus Laminated
684 Layer Inhibit CD40 Upregulation in Dendritic Cells by Interfering with Akt
685 Activation. Infect Immun 87:e00641-19.

686 12. Casaravilla C, Pittini A, Rückerl D, Seoane PI, Jenkins SJ, MacDonald AS,
687 Ferreira AM, Allen JE, Díaz A. 2014. Unconventional maturation of dendritic cells
688 induced by particles from the laminated layer of larval Echinococcus granulosus.
689 Infect Immun 82:3164–3176.

690 13. Hsu T-L, Lin G, Koizumi A, Brehm K, Hada N, Chuang P-K, Wong C-H, Hsieh
691 S-L, Díaz A. 2013. The surface carbohydrates of the Echinococcus granulosus

692 larva interact selectively with the rodent Kupffer cell receptor. Molecular and
693 Biochemical Parasitology 192:55–59.

694 14. Fadden AJ, Holt OJ, Drickamer K. 2003. Molecular characterization of the rat
695 Kupffer cell glycoprotein receptor. Glycobiology 13:529–537.

696 15. Taylor ME, Snelling T, Smith DF, Drickamer K. 2019. Absence of a human
697 ortholog of rodent Kupffer cell galactose-binding receptor encoded by the CLEC4f
698 gene. Glycobiology 29:332–345.

699 16. Yang C-Y, Chen J-B, Tsai T-F, Tsai Y-C, Tsai C-Y, Liang P-H, Hsu T-L, Wu C-
700 Y, Netea MG, Wong C-H, Hsieh S-L. 2013. CLEC4F Is an Inducible C-Type
701 Lectin in F4/80-Positive Cells and Is Involved in Alpha-Galactosylceramide
702 Presentation in Liver. PLoS ONE 8:e65070.

703 17. Coombs PJ, Taylor ME, Drickamer K. 2006. Two categories of mammalian
704 galactose-binding receptors distinguished by glycan array profiling. Glycobiology
705 16:1C-7C.

706 18. Ouyang Z, Felix J, Zhou J, Pei Y, Ma B, Hwang PM, Lemieux MJ, Gutsche I,
707 Zheng F, Wen Y. 2020. Trimeric structure of the mouse Kupffer cell C-type lectin
708 receptor Clec4f. FEBS Lett 594:189–198.

709 19. Jiang Y, Tang Y, Hoover C, Kondo Y, Huang D, Restagno D, Shao B, Gao L,
710 Michael McDaniel J, Zhou M, Silasi-Mansat R, McGee S, Jiang M, Bai X, Lupu
711 F, Ruan C, Marth JD, Wu D, Han Y, Xia L. 2021. Kupffer cell receptor CLEC4F
712 is important for the destruction of desialylated platelets in mice. Cell Death Differ
713 28:3009–3021.

714 20. Deppermann C, Kratofil RM, Peiseler M, David BA, Zindel J, Castanheira FVES,
715 van der Wal F, Carestia A, Jenne CN, Marth JD, Kubes P. 2020. Macrophage
716 galactose lectin is critical for Kupffer cells to clear aged platelets. J Exp Med
717 217:e20190723.

718 21. Li Y, Fu J, Ling Y, Yago T, McDaniel JM, Song J, Bai X, Kondo Y, Qin Y,
719 Hoover C, McGee S, Shao B, Liu Z, Sonon R, Azadi P, Marth JD, McEver RP,
720 Ruan C, Xia L. 2017. Sialylation on O-glycans protects platelets from clearance by
721 liver Kupffer cells. Proc Natl Acad Sci USA 114:8360–8365.

722 22. Heymann F, Peusquens J, Ludwig-Portugall I, Kohlhepp M, Ergen C, Niemietz P,
723 Martin C, van Rooijen N, Ochando JC, Randolph GJ, Luedde T, Ginhoux F, Kurts
724 C, Trautwein C, Tacke F. 2015. Liver inflammation abrogates immunological
725 tolerance induced by Kupffer cells. Hepatology 62:279–291.

726 23. Rothlin CV, Carrera-Silva EA, Bosurgi L, Ghosh S. 2015. TAM receptor signaling
727 in immune homeostasis. Annu Rev Immunol 33:355–391.

728 24. Casaravilla C, Díaz A. 2010. Studies on the structural mucins of the Echinococcus
729 granulosus laminated layer. Molecular and Biochemical Parasitology 174:132–
730 136.

731 25. (1) Committee for the update of the guide for the care and use of laboratory
732 animals. 2011. Guide for the care and use of laboratory animals, 8th ed. National
733 Academies Press.

734 26. Meikle MN, Schlapp G, Menchaca A, Crispo M. 2018. Minimum volume Spatula
735 MVD vitrification method improves embryo survival compared to traditional slow

736 freezing, both for in vivo and in vitro produced mice embryos. Cryobiology
737 84:77–81.

738 27. Schlapp G, Goyeneche L, Fernández G, Menchaca A, Crispo M. 2015.
739 Administration of the nonsteroidal anti-inflammatory drug tolfenamic acid at
740 embryo transfer improves maintenance of pregnancy and embryo survival in
741 recipient mice. J Assist Reprod Genet 32:271–275.

742 28. Barth TFE, Herrmann TS, Tappe D, Stark L, Grüner B, Buttenschoen K,
743 Hillenbrand A, Juchems M, Henne-Bruns D, Kern P, Seitz HM, Möller P, Rausch
744 RL, Kern P, Deplazes P. 2012. Sensitive and Specific Immunohistochemical
745 Diagnosis of Human Alveolar Echinococcosis with the Monoclonal Antibody
746 Em2G11. PLoS Negl Trop Dis 6:e1877.

747 29. Baz A, Richieri A, Puglia A, Nieto A, Dematteis S. 1999. Antibody response in
748 CD4-depleted mice after immunization or during early infection with
749 Echinococcus granulosus. Parasite Immunol 21:141–150.

750 30. Hsu T-L, Cheng S-C, Yang W-B, Chin S-W, Chen B-H, Huang M-T, Hsieh S-L,
751 Wong C-H. 2009. Profiling carbohydrate-receptor interaction with recombinant
752 innate immunity receptor-Fc fusion proteins. J Biol Chem 284:34479–34489.

753 31. Hollander M, Wolfe DE, Chicken E. 2015. Nonparametric Statistical Methods, 3rd
754 ed. John Wiley & Sons, New York.

755 32. Lynch RW, Hawley CA, Pellicoro A, Bain CC, Iredale JP, Jenkins SJ. 2018. An
756 efficient method to isolate Kupffer cells eliminating endothelial cell contamination
757 and selective bias. J Leukoc Biol 104:579–586.

758 33. Cummings RD, Etzler, ME. Antibodies and lectins in glycan analysis, p. 633–647.
759 *In* Essentials of GlycobiologySecond Edition. Cold Spring Harbor Laboratory
760 Press.

761 34. Dematteis S, Pirotto F, Marqués J, Nieto A, Orn A, Baz A. 2001. Modulation of
762 the cellular immune response by a carbohydrate rich fraction from Echinococcus
763 granulosus protoscoleces in infected or immunized Balb/c mice. Parasite Immunol
764 23:1–9.

765 35. Walker M, Baz A, Dematteis S, Stettler M, Gottstein B, Schaller J, Hemphill A.
766 2004. Isolation and characterization of a secretory component of Echinococcus
767 multilocularis metacestodes potentially involved in modulating the host-parasite
768 interface. Infect Immun 72:527–536.

769 36. Araj GF, Matossian RM, Frayha GJ. 1977. The host response in secondary
770 hydatidosis of mice. I. Circulating antibodies. Z Parasitenkd 52:23–30.

771 37. Richards KS, Arme C, Bridges JF. 1983. Echinococcus granulosus equinus: an
772 ultrastructural study of murine tissue response to hydatid cysts. Parasitology 86 (Pt
773 3):407–417.

774 38. Mourglia-Ettlin G, Cucher M, Arbildi P, Rosenzvit M, Dematteis S. 2016. Natural
775 and induced antibodies contribute to differential susceptibility to secondary cystic
776 echinococcosis of Balb/c and C57Bl/6 mice. Immunobiology 221:103–115.

777 39. Raedler A, Raedler E, Arndt R, Thiele HG. 1981. Terminal galactosyl residues of
778 cell-surface glycoconjugates exposed on both human and murine immature T- and
779 B-cells. Cell Tissue Res 218:219–226.

780 40. Díaz A, Allen JE. 2007. Mapping immune response profiles: The emerging
781 scenario from helminth immunology. Eur J Immunol 37:3319–3326.

782 41. Wang J, Kubes P. 2016. A Reservoir of Mature Cavity Macrophages that Can
783 Rapidly Invade Visceral Organs to Affect Tissue Repair. Cell 165:668–678.

784 42. Grewal PK. 2010. The Ashwell–Morell Receptor, p. 223–241. *In* Methods in
785 Enzymology. Elsevier.

786 43. Rensen PC, Sliedregt LA, Ferns M, Kieviet E, van Rossenberg SM, van Leeuwen
787 SH, van Berkel TJ, Biessen EA. 2001. Determination of the upper size limit for
788 uptake and processing of ligands by the asialoglycoprotein receptor on hepatocytes
789 in vitro and in vivo. J Biol Chem 276:37577–37584.

790 44. Barrios AA, Grezzi L, Miles S, Mariconti M, Mourglia-Ettlin G, Seoane PI, Díaz
791 A. 2019. Inefficient and abortive classical complement pathway activation by the
792 calcium inositol hexakisphosphate component of the Echinococcus granulosus
793 laminated layer. Immunobiology 224:710–719.

794 45. Irigoín F, Ferreira F, Fernández C, Sim RB, Díaz A. 2002. myo-Inositol
795 hexakisphosphate is a major component of an extracellular structure in the
796 parasitic cestode Echinococcus granulosus 8.

797 46. Irigoín F, Casaravilla C, Iborra F, Sim RB, Ferreira F, Díaz A. 2004. Unique
798 precipitation and exocytosis of a calcium salt of *myo* -inositol hexakisphosphate in
799 larval *Echinococcus granulosus*. J Cell Biochem 93:1272–1281.

800 47. Casaravilla C, Brearley C, Soule S, Fontana C, Veiga N, Bessio MI, Ferreira F,
801 Kremer C, Diaz A. 2006. Characterization of myo-inositol hexakisphosphate
802 deposits from larval Echinococcus granulosus. FEBS Journal 273:3192–3203.

803 48. Irigoín F, Laich A, Ferreira AM, Fernández C, Sim RB, Díaz A. 2008. Resistance
804 of the Echinococcus granulosus cyst wall to complement activation: analysis of the
805 role of $InsP_6$ deposits. Parasite Immunol 30:354–364.

806 49. Seoane PI, Rückerl D, Casaravilla C, Barrios AA, Pittini Á, MacDonald AS, Allen
807 JE, Díaz A. 2016. Particles from the Echinococcus granulosus laminated layer
808 inhibit IL-4 and growth factor-driven Akt phosphorylation and proliferative
809 responses in macrophages. Sci Rep 6:39204.

810 50. Casaravilla C, Pittini Á, Rückerl D, Allen JE, Díaz Á. 2020. Activation of the
811 NLRP3 Inflammasome by Particles from the Echinococcus granulosus Laminated
812 Layer. Infect Immun 88.

813 51. Lüth S, Huber S, Schramm C, Buch T, Zander S, Stadelmann C, Brück W, Wraith
814 DC, Herkel J, Lohse AW. 2008. Ectopic expression of neural autoantigen in
815 mouse liver suppresses experimental autoimmune neuroinflammation by inducing
816 antigen-specific Tregs. J Clin Invest 118:3403–3410.

817 52. You Q, Cheng L, Kedl RM, Ju C. 2008. Mechanism of T cell tolerance induction
818 by murine hepatic Kupffer cells. Hepatology 48:978–990.

819 53. Hoberg EP, Jones A, Rausch RL, Eom KS, Gardner SL. 2000. A phylogenetic
820 hypothesis for species of the genus Taenia (Eucestoda : Taeniidae). J Parasitol
821 86:89–98.

822 54. del Puerto L, Rovetta R, Navatta M, Fontana C, Lin G, Moyna G, Dematteis S,
823 Brehm K, Koziol U, Ferreira F, Díaz A. 2016. Negligible elongation of mucin
824 glycans with Gal β1-3 units distinguishes the laminated layer of Echinococcus
825 multilocularis from that of Echinococcus granulosus. International Journal for
826 Parasitology 46:311–321.

827 55. Basika T, Muñoz N, Casaravilla C, Irigoín F, Batthyány C, Bonilla M, Salinas G,
828 Pacheco JP, Roth J, Durán R, Díaz A. 2012. Phagocyte-specific S100 proteins in
829 the local response to the *Echinococcus granulosus* larva. Parasitology 139:271–
830 283.

831

832

833 **Figure legends**

834

835 **Fig. 1. Soluble LL mucins are taken up selectively by KC, dependent on mucin glycans.**
836 C57BL/6 mice were injected i.v. with 100 µg dry mass of solubilized, biotin-derivatized LL
837 mucins (sLL), either treated with periodate to oxidize their terminal monosaccharide residues
838 or mock-treated. Twenty minutes later, mice were sacrificed and sLL uptake was quantitated
839 in permeabilized liver non parenchymal cells using streptavidin-PE. Data are shown for the
840 cell types that are relevant in the context of the article, namely KC, LSEC and non-KC
841 $CD11b^+$ cells, in terms of percentages of positive cells **(a)** and geometric means of
842 fluorescence intensity **(b)**. Representative dot-plots for KC are shown in **(c)**. The signal
843 threshold for each cell type was established using cells from mice injected with vehicle only
844 and similarly stained; the fluorescence intensities data had the median values corresponding
845 to vehicle-injected mice subtracted for plotting. Results are pooled from 3 independent
846 experiments (represented in different colours); individual mice and their overall median
847 values are shown. The statistical analyses were carried out on the crude data, by the Mack-
848 Skillings test.

849

850 **Fig. 2. PNA and the E492 antibody are suitable probes for LL mucins captured by**
851 **mouse KC.** The binding of PNA, the E492 antibody and soluble recombinant Clec4F to
852 LL mucins coated onto ELISA plate wells **(a)** or present in LL particles in suspension **(b)**
853 was studied. The capacity of PNA and the E492 antibody to compete with the binding of
854 recombinant Clec4F to LL mucins was analysed in a competition ELISA format **(c)**;
855 results are expressed in relation to the response in the absence of competitor. In (a) and
856 (c), analytical duplicates are shown. WT C57BL/6 mice were injected i.v. either with PBS
857 only or with solubilized LL mucins (200 µg/mouse) and 22 h later KC and LSEC were

858 analysed by flow cytometry using either PNA or the E492 antibody as probes, after cell
859 permeabilization (**d**). Staining controls shown in (b) and (d) correspond to samples
860 stained in the same way as the positive ones except that the primary probe for LL material
861 was omitted, and the analogous controls in (a) gave no signal.
862
863 **Fig. 3. Generation of Clec4f gene-deficient mice. (a)** Schematic structure of the mouse
864 *Clec4f* gene. Coding exons appear as solid black bars and non-coding regions as white
865 bars. Introns are represented as lines. **(b)** The target sequences for CRISPR/Cas9, 5'-
866 TGGACGTGCCGCAGGGTCCT-3' and 5'-GCTTCTCCCCTGCAGGACTG-3', are
867 located in the second exon and first intron/second exon junction of the gene respectively.
868 An 8 bp deletion corresponding to nucleotides 5'- CAGGACCC-3' was identified by tail
869 biopsy. The frameshift mutation produces a protein 480 aa shorter. **(c)** The liver non-
870 parenchymal fraction was prepared from Clec4f$^{-/-}$ and WT mice and analyzed for Clec4F
871 expression by flow cytometry without or with cellular permeabilization. KC were defined
872 as shown in Figure S2. The staining controls contain all the fluorophore-coupled
873 antibodies but lack the primary anti-Clec4F antibody.
874
875 **Fig. 4. Fast uptake of soluble LL mucins by Kupffer cells depends largely on Clec4F.**
876 WT and Clec4f$^{-/-}$ mice were injected i.v. with 200 ug dry mass of sLL, either untreated or
877 mock-treated as in Figure 1, or vehicle only (PBS). Twenty min later, mice were sacrificed
878 and sLL uptake was quantitated in non-parenchymal liver cell populations by flow cytometry
879 in permeabilized cells using PNA. Results are shown for KC, LSEC and non-KC CD11b^{+}
880 cells, in terms of percentages of positive cells **(a)** and mean fluorescence intensities **(b)**, and
881 representative flow cytometry plots are shown for KC and LSEC **(c)**. An estimation of the
882 fraction of sLL taken up by each of the cell populations under study, calculated as explained

883 in the Materials and Methods section, is shown in **(d)**; the statistics shown compare the
884 fractions taken up by KC. The positive cell threshold was established using cells from the
885 mice injected with PBS only. The data arise from two independent experiments, represented
886 in blue and red in (a-c) and indicated as 1, 2 in (d). In (a-c), individual mice and their median
887 values, and in (d) only medians, are shown. The statistical analyses were carried out by the
888 Mack-Skillings test.
889
890 **Fig. 5. Clec4F is important for the capture of soluble LL mucins by Kupffer cells even**
891 **after allowing a long uptake time.** WT and Clec4f$^{-/-}$ C57BL/6 mice were injected i.v. with
892 200 μg dry mass per mouse of sLL (mock-treated as in Fig. 1) or PBS only as a control.
893 Twenty-two h later, mice were sacrificed and sLL uptake was quantitated in liver non-
894 parenchymal cells by flow cytometry using PNA after cell permeabilization. Results are
895 shown for KC, LSEC and non-KC CD11b^{+} cells, in terms of percentages of positive cells **(a)**
896 and mean fluorescence intensities **(b)**, and representative flow plots for KC and LSEC are
897 shown in **(c)**. An estimation of the fraction of sLL taken up by each of the cell populations
898 under study, calculated as explained in the Materials and Methods section, is shown in **(d);**
899 the statistics shown compare the fractions taken up by KC. The positive cell threshold was
900 established using staining controls (in which only biotinylated PNA was omitted). The PNA
901 signal in non-permeabilized cells was negligible. The data arise from two independent
902 experiments, represented in blue and red in (a-c) and indicated as 1, 2 in (d). In (a-c),
903 individual mice and their median values, and in (d) only medians, are shown. The statistical
904 analyses were carried out by the Mack-Skillings test (a-c) and the modified Wilcoxon-Mann-
905 Whitney tests (d).
906

907 **Fig. 6. The uptake by Kupffer cells of LL mucins injected in particulate presentation**
908 **depends largely on Clec4F.** WT and Clec4f$^{-/-}$ C57BL/6 mice were injected i.p. with 450 µg
909 dry mass of pLL or PBS only as a control. Twenty-two h later, mice were sacrificed and pLL
910 uptake was quantitated in liver non-parenchymal cells by flow cytometry using PNA after
911 cell permeabilisation. Results are shown for KC, LSEC and non-KC CD11b^{+} cells, in terms
912 of percentages of positive cells **(a)** and mean fluorescence intensities **(b)**, and representative
913 dot-plots for the three cell types are shown in **(c)**. An estimation of the fraction of sLL taken
914 up by each of the cell populations under study, calculated as explained in the Materials and
915 Methods section, is shown in **(d)**; the statistics shown compare the fractions taken up by KC..
916 The positive cell threshold was established using staining controls. The data arise from two
917 independent experiments, represented in blue and red in (a-c) and indicated as 1, 2 in (d). In
918 (a-c), individual mice and their median values, and in (d) only medians, are shown. The
919 statistical analyses were carried out by the Mack-Skillings test. The analogous flow
920 cytometry results obtained using the E492 antibody for detection are shown in Fig. S6. In
921 addition, pLL was detected in liver sections, using the E492 antibody (**e**). Representative
922 images are shown, at two different magnifications. Black arrows indicate KC-like cells
923 staining strongly for LL material; empty arrowheads indicate hepatocytes staining weakly for
924 LL material.
925
926 **Fig. 7. LL materials circulate systemically in infected mice and are captured selectively**
927 **by Kupffer cells via Clec4F.** BALB/c mice (WT) were intraperitoneally infected with *E.*
928 *granulosus* protoscoleces or injected with the corresponding volume of buffer only. Seven
929 months later, the presence of LL-derived materials in various organs was analysed by
930 histology, using the E492 antibody as a probe **(a)**. Images from representative mice are
931 shown, out of 15 infected and 5 control mice; the bars represent 50 µm. Black arrows indicate

932 KC-like cells staining for LL material; empty arrowheads indicate occasional staining for LL
933 material in spleen and lymph node. The staining observed in adipocytes (upper left-hand
934 corner of the infected mouse mesenteric lymph node section) was also observed in adipocytes
935 present in kidney and lung sections, irrespective of infection, and must therefore represent a
936 cross-reaction of the antibody. No staining was observed in sections probed with the
937 secondary reagent only. The uptake of LL-derived materials by non-parenchymal liver cells
938 of infected BALB/c mice was also analysed by flow cytometry, using PNA as probe. Results
939 are shown for KC, LSEC and non-KC $CD11b^{+}$ cells, in terms of percentages of positive cells
940 **(b)** and mean fluorescence intensities **(c)**, and representative dot-plots for the three cell types
941 are shown in **(d)**. The positive cell threshold was established using staining controls. In
942 addition, WT and $Clec4f^{-/-}$ C57BL/6 mice were similarly infected and the uptake of LL-
943 derived materials analysed by flow cytometry and presented **(e – g)** as for the BALB/c mice.
944 Results in (a – d) are from a single experiment and results in (e - g) are pooled from two
945 independent experiments, shown in blue and red. In (b - g), data shown correspond to
946 individual mice and their median values are indicated. The statistical analyses were carried
947 out by the modified Wilcoxon-Mann-Whitney (b, c) and Kruskal-Wallis tests (e, g).
948
949 **Supplementary Figures.**
950
951 **Fig. S1. Summary of preparation of LL materials.** The preparation of pLL and sLL
952 (periodate- or mock-treated) is summarized in **(a)**. Periodate oxidation of terminal
953 monosaccharides and further monosaccharides carrying *cis*-diols generates reactive aldehyde
954 groups, which are reduced to alcohols using sodium borohydride. The mock treatment
955 consists of the borohydride step only. The effectiveness of the periodate treatment was
956 verified in terms of abrogation of PNA binding by to the mucins in a dot-blot format **(b)**.

957 Similar incorporation of the biotin tag to periodate- and mock-treated sLL was verified using
958 streptavidin-peroxidase in dot-blot format **(c)**.
959
960 **Fig. S2. Gating strategy for liver cells.** Gating strategies are shown for KC, LSEC, and non-
961 KC CD11b$^+$ cells. For non-KC CD11b$^+$ cells, which tend to be substantially smaller than KC,
962 it was necessary to include an additional doublet exclusion step at the end of the gating
963 strategy.
964
965 **Fig. S3 (related to Fig. 3). Reactivity of PNA, E492 antibody and recombinant Clec4F**
966 **with liver non-parenchymal cells of control mice.** Non-parenchymal cells from WT
967 C57BL/6 mice were stained for flow cytometry with PNA, E492 antibody or recombinant
968 mouse Clec4F, followed by appropriate secondary probes. The staining controls correspond
969 to samples stained in the same way as the positive ones except that the primary probe was
970 omitted.
971
972 **Fig. S4 (related to Figs. 4 and 5). Representative flow plots for liver non-KC CD11b$^+$**
973 **cells.** sLL was injected in WT and Clec4f$^{-/-}$ C57BL/6 mice, and liver non parenchymal cells
974 analysed after 20 min **(a)** or 22 h **(b)**, as described in Figs. 4 and 5 respectively. Representative
975 flow plots are shown for non-KC CD11b$^+$ cells, which were not found to take up sLL
976 significantly.
977
978 **Fig. S5 (related to Fig. 5). Surface expression of Clec4F does not change upon injection**
979 **of sLL.** WT C57BL/6 mice were injected with sLL or vehicle only (PBS) as described in Fig.
980 5, and 22 h later KC were analysed for surface expression of Clec4F by flow cytometry. Data
981 shown, in terms of geometric means of fluorescence intensity (MFI), arise from 3

982 independent experiments, shown in different colors. The data were normalized over the
983 median value of mice injected with PBS only in each experiment.
984
985 **Fig. S6 (related to Fig. 6). Uptake of pLL by liver non-parenchymal cells measured by**
986 **flow cytometry using antibody E492.** WT and Clec4f$^{-/-}$ C57BL/6 mice were injected with
987 pLL and material uptake was analysed as in Figure 6 except that the E492 antibody was used
988 as probe. Results are shown in terms of percentages of positive cells **(a)** and mean
989 fluorescence intensities **(b)**, and representative dot-plots are shown in **(c)**. An estimation of
990 the fraction of sLL taken up by each of the cell populations under study, calculated as
991 explained in the Materials and Methods section, is shown in **(d)**; the statistics shown compare
992 the fractions taken up by KC. The positive cell threshold was established using staining
993 controls. The data arise from two independent experiments, represented in blue and red in (a-
994 c) and indicated as 1, 2 in (d). In (a-c), individual mice and their median values, and in (d)
995 only medians, are shown. The statistical analyses were carried out by the Mack-Skillings test.
996
997 **Fig. S7 (related to Fig. 6). Frequency of non-KC CD11b^{+} cells in mice injected with pLL.**
998 WT and Clec4f$^{-/-}$ C57BL/6 mice were injected with pLL or vehicle only (PBS) as described
999 in Fig. 6, and 22 h later the frequency of non-KC CD11b^{+} cells within all live cells was
1000 measured by flow cytometry. Data arise from 2 independent experiments, shown in different
1001 colors.
1002
1003 **Fig. S8 (related to Fig. 6). Surface expression of Clec4F does not change upon injection**
1004 **of pLL.** WT C57BL/6 mice were injected with pLL or vehicle only (PBS) as described in
1005 Fig. 6, and 22 h later KC were analysed for surface expression of Clec4F by flow cytometry.
1006 Data shown, in terms of geometric means of fluorescence intensity (MFI), arise from 2

1007 independent experiments, shown in different colors. The data were normalized over the
1008 median value of mice injected with PBS only in each experiment.
1009
1010 **Fig. S9 (related to Fig. 7). Parasite burdens of mice infected with *E. granulosus*.** WT
1011 BALB/c mice **(a)** or WT and Clec4f$^{-/-}$ C57BL/6 mice **(b)** were infected with *E. granulosus*
1012 as described in Fig. 7. Parasite burdens are expressed in terms of total volumes of
1013 metacestodes, measured by water displacement. Results for BALB/c mice correspond to a
1014 single experiment and results for C57BL/6 are pooled from 2 experiments, represented in
1015 different colours. Individual mice and their overall median values are shown. Parasite burdens
1016 were not found to be significantly different between WT and Clec4f$^{-/-}$ C57BL/6 mice by the
1017 Kruskall-Wallis test.
1018
1019 **Fig. S10 (related to Fig. 7). Representative flow plots for LSEC in infections.** WT
1020 BALB/c mice **(a)** or WT and Clec4f$^{-/-}$ C57BL/6 mice **(b)** were infected with *E. granulosus*
1021 and liver non-parenchymal cells analysed by flow cytometry as described in Fig. 7.
1022 Representative flow plots are shown for LSEC, which were not found to take up LL materials.
1023
1024 **Fig. S11. Frequencies of non-KC CD11b^{+} cells in *E. granulosus* experimental infections.**
1025 WT BALB/c mice **(a)** or WT and Clec4f$^{-/-}$ C57BL/6 mice **(b)** were infected with *E.*
1026 *granulosus* and liver non-parenchymal cells analysed by flow cytometry as described in Fig.
1027 7. Frequencies of non-KC CD11b^{+} cells within total live cells are plotted. The statistical
1028 analysis was carried out by the modified Wilcoxon-Mann-Whitney method.
1029
1030 **Fig. S12. Experimental *E. granulosus* infection does not alter the expression of Clec4F**
1031 **in KC.** WT BALB/c mice **(a)** or WT C57BL/6 mice **(b)** were infected with *E. granulosus* as

1032 described in Fig. 7. KC were analysed for surface expression of Clec4F by flow cytometry.
1033 Data shown, in terms of geometric means of fluorescence intensity (MFI), arise from 1
1034 experiment for each of the mouse strains shown. The data were normalized over the median
1035 value of the control mice in each experiment.
1036

FIGURE 1

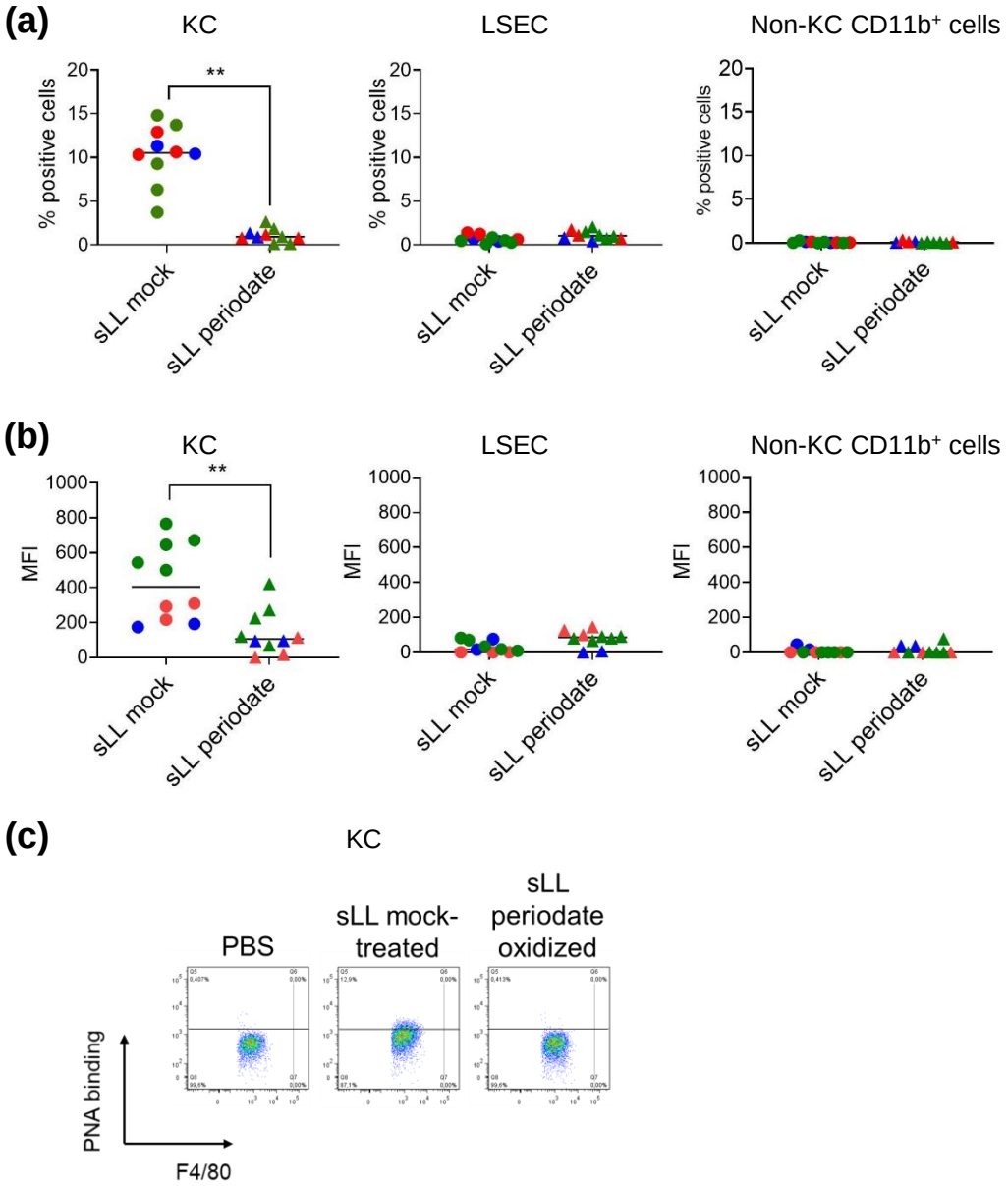
(a)
KC
LSEC
Non-KC CD11b+ cells
% positive cells
**
sLL mock
sLL periodate
(b)
MFI
(c)
PBS
sLL mock-treated
sLL periodate oxidized
PNA binding
F4/80

FIGURE 2

(a) ELISA format

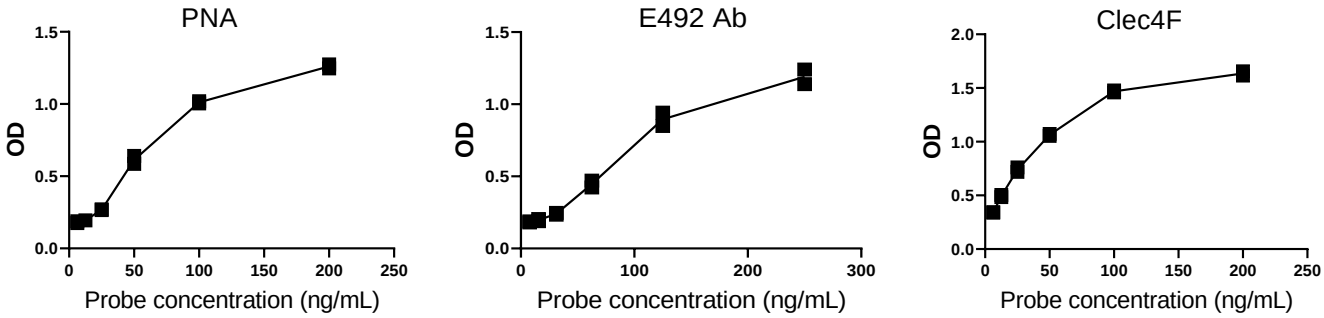

(b) Immuno/lectin fluorescence on particles

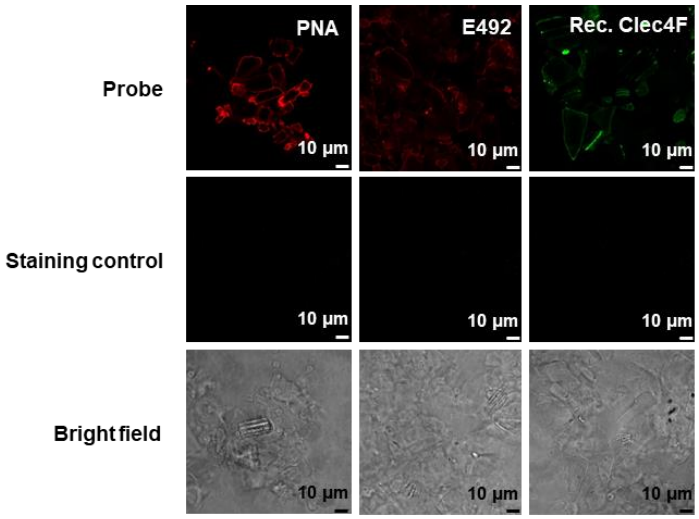

(c) Competition ELISA format

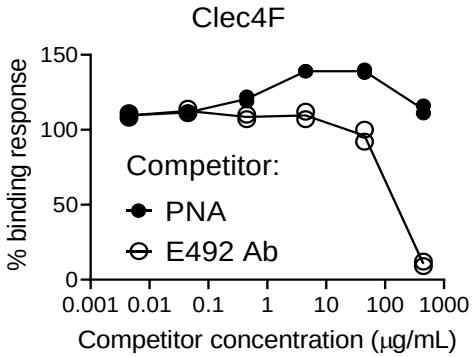

(d) Flow cytometry gated on KC and LSEC

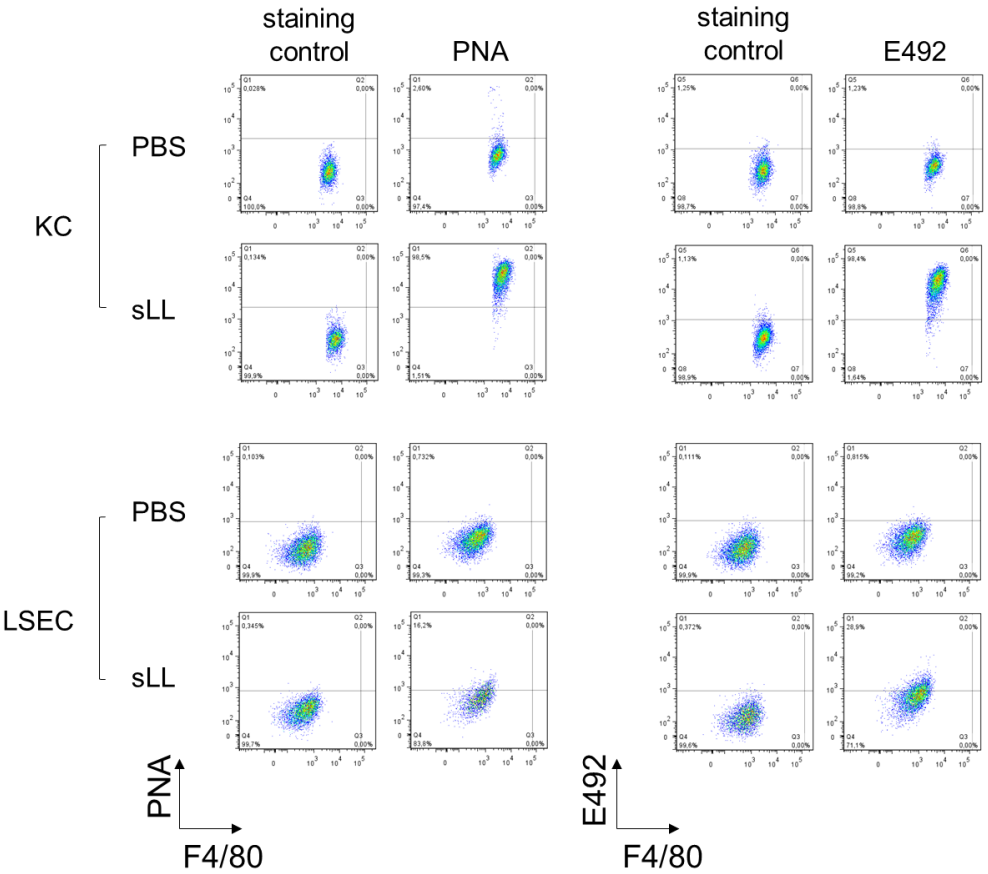

FIGURE 3

(a)

Mus musculus clec4f (Chr. 6)

ENSMUST00000014686.3

(b)

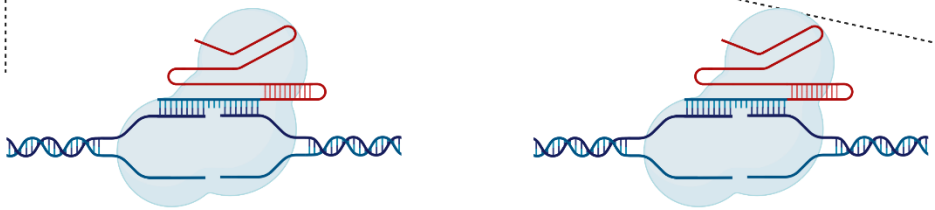

(c)

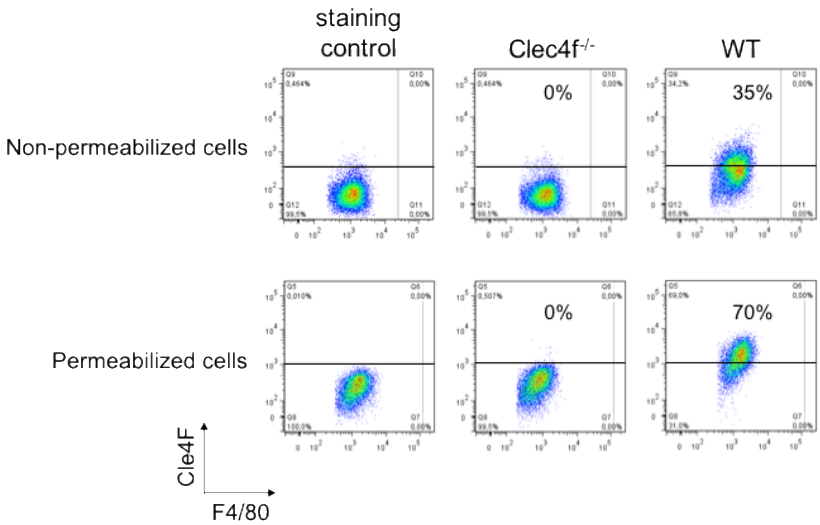

FIGURE 4

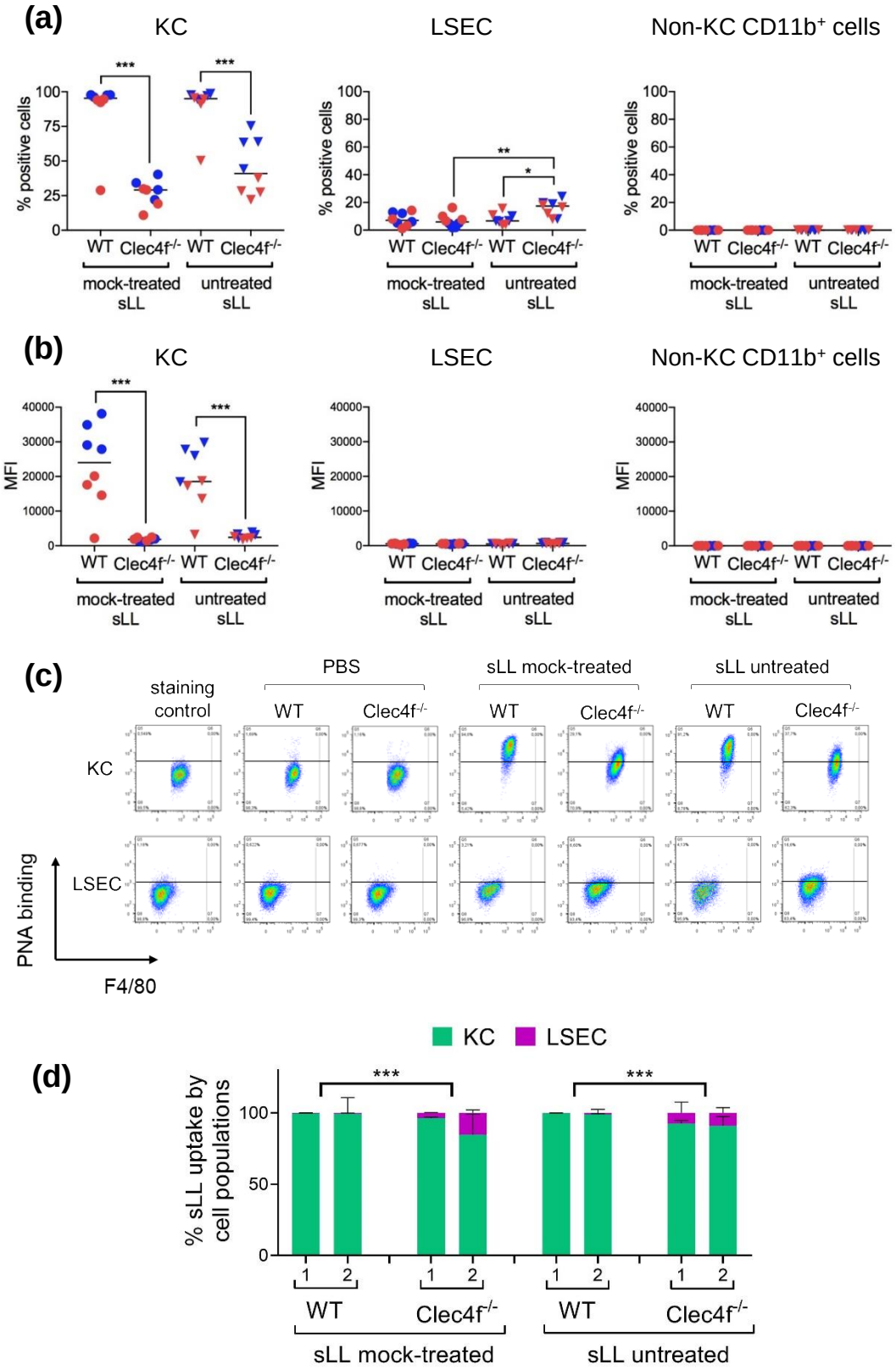
(a)
KC
LSEC
Non-KC CD11b+ cells
% positive cells
***
**
*
WT
Clec4f-/-
mock-treated sLL
untreated sLL
(b)
MFI
(c)
staining control
PBS
sLL mock-treated
sLL untreated
KC
LSEC
PNA binding
F4/80
(d)
% sLL uptake by cell populations
sLL mock-treated
sLL untreated

Figure 5

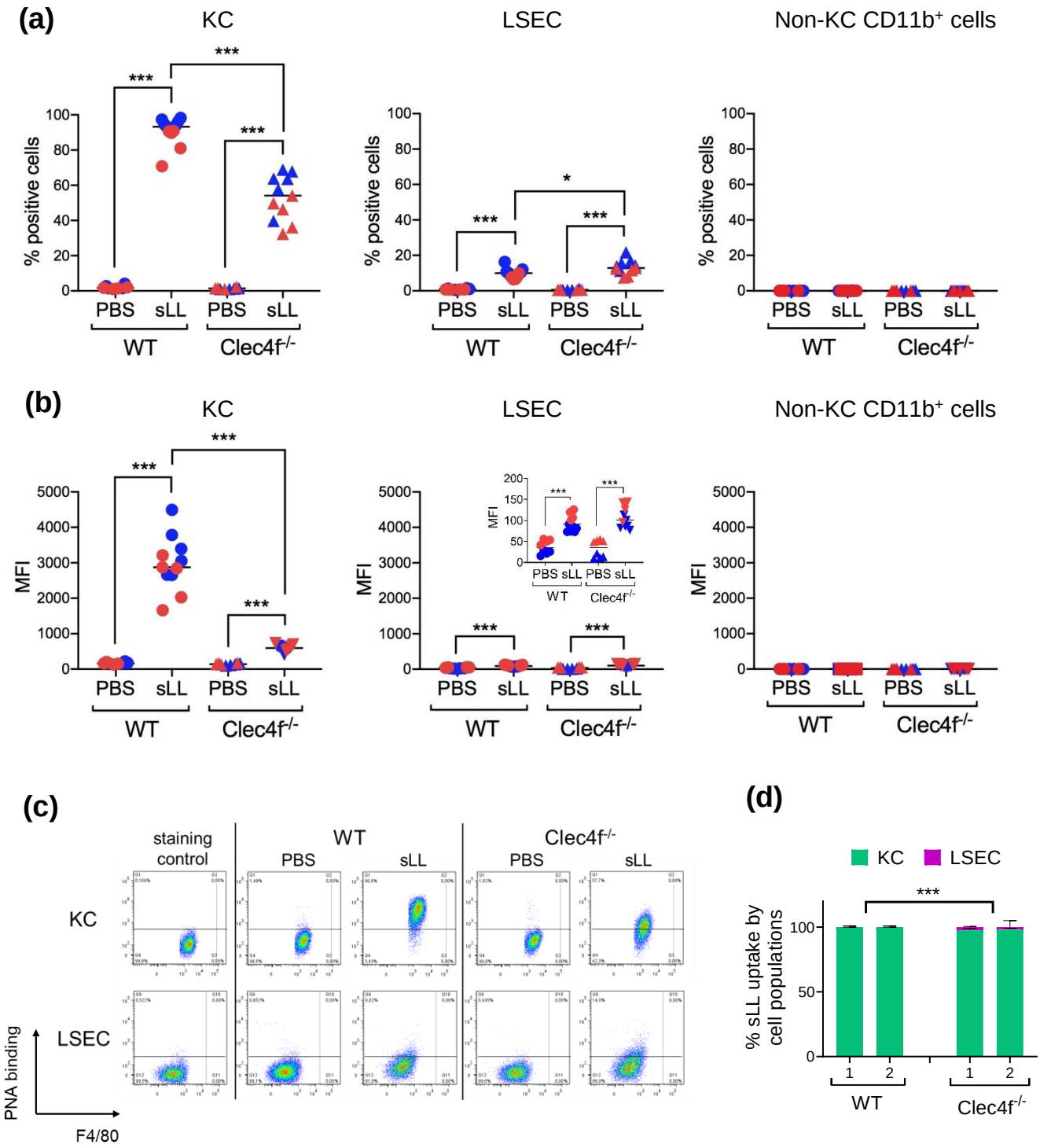
(a)
KC
LSEC
Non-KC CD11b+ cells
% positive cells
PBS
sLL
WT
Clec4f-/-
(b)
MFI
(c)
staining control
WT
Clec4f-/-
PBS
sLL
KC
LSEC
PNA binding
F4/80
(d)
KC
LSEC
% sLL uptake by cell populations

Figure 6

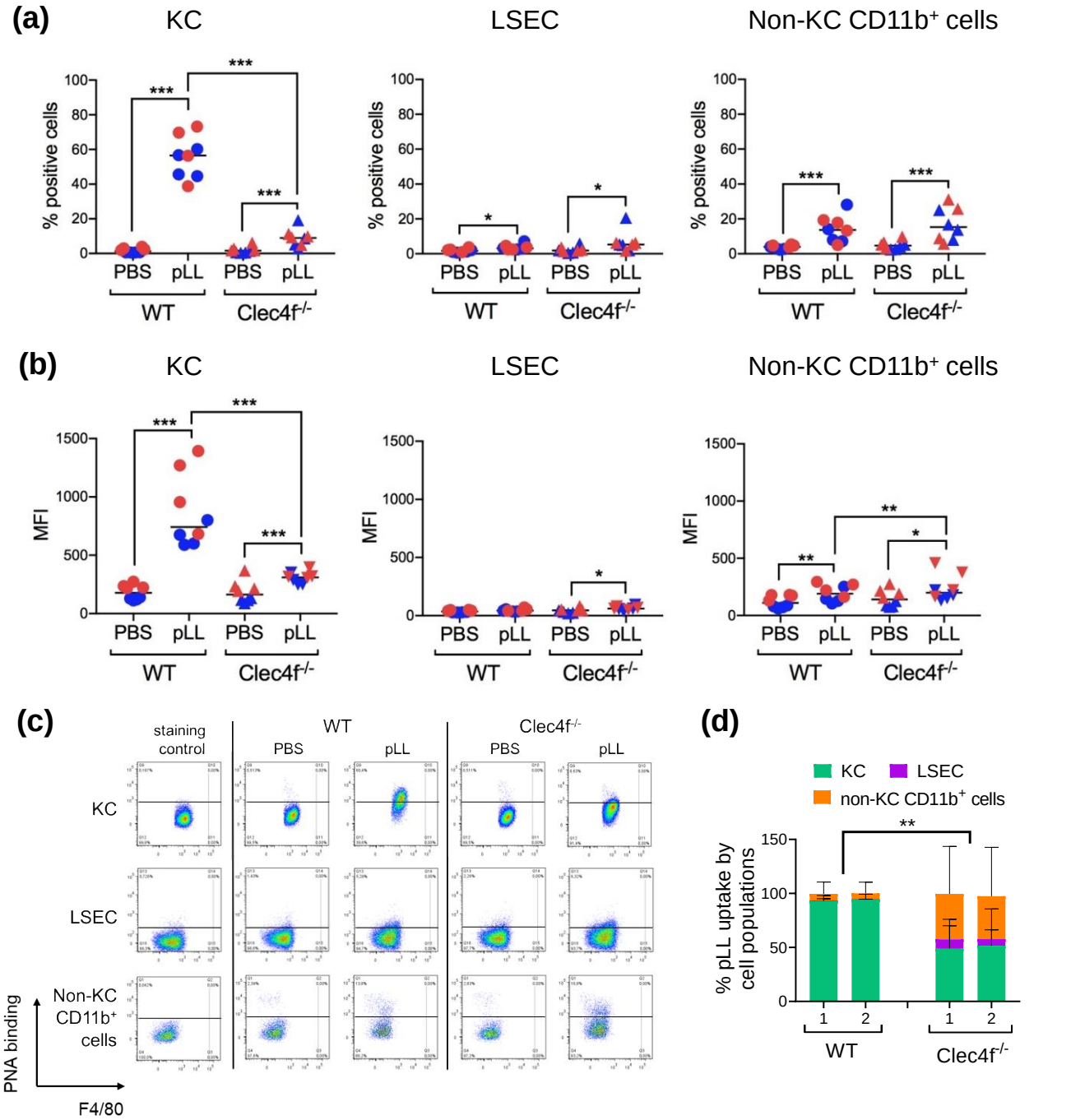
(a)
KC
LSEC
Non-KC CD11b+ cells
% positive cells
PBS
pLL
WT
Clec4f-/-
(b)
MFI
(c)
staining control
WT
Clec4f-/-
KC
LSEC
Non-KC CD11b+ cells
PNA binding
F4/80
(d)
KC
LSEC
non-KC CD11b+ cells
% pLL uptake by cell populations

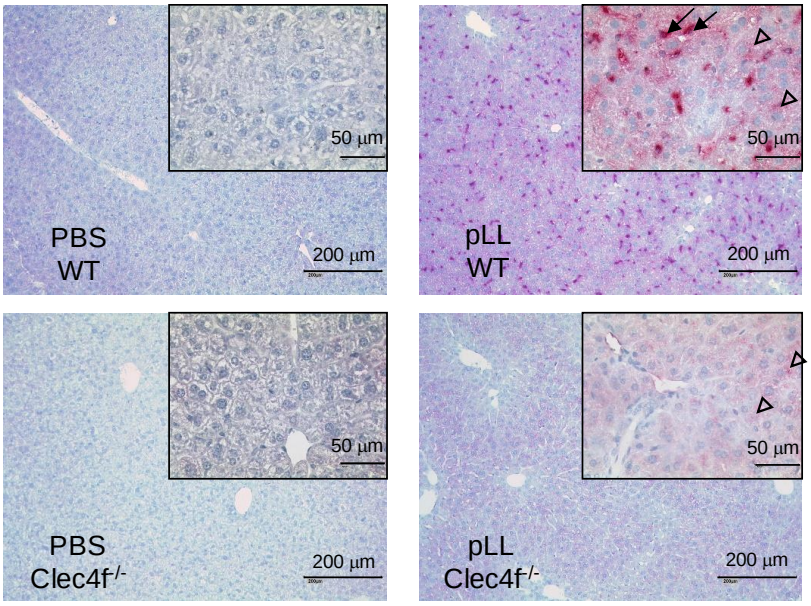
(e)
PBS WT
pLL WT
PBS Clec4f-/-
pLL Clec4f-/-
50 µm
200 µm

Figure 7

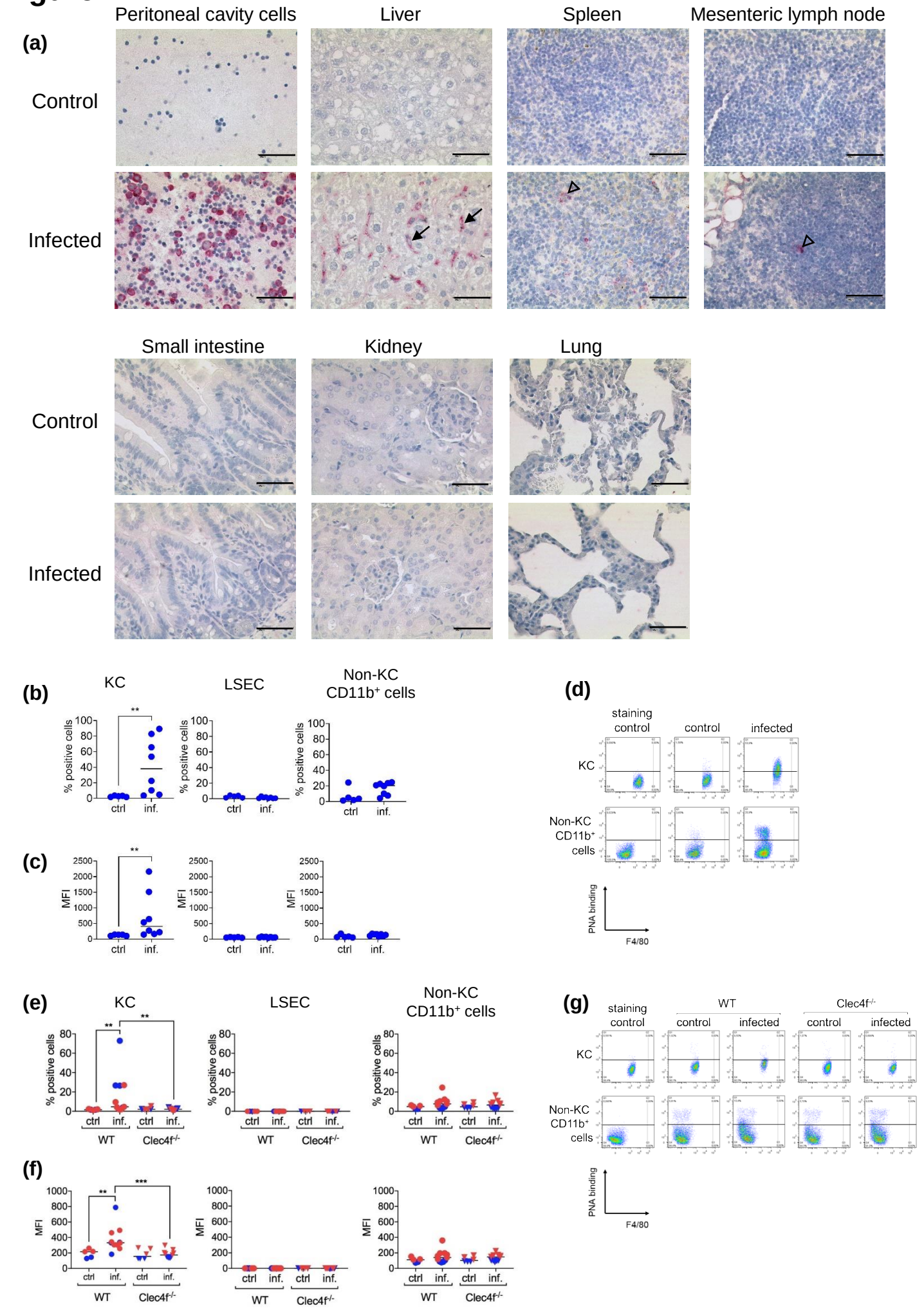
(a)
Peritoneal cavity cells
Liver
Spleen
Mesenteric lymph node
Control
Infected
Small intestine
Kidney
Lung
Control
Infected
(b)
KC
LSEC
Non-KC CD11b+ cells
% positive cells
ctrl
inf.
(c)
MFI
(d)
staining control
control
infected
KC
Non-KC CD11b+ cells
PNA binding
F4/80
(e)
KC
LSEC
Non-KC CD11b+ cells
% positive cells
ctrl
inf.
WT
Clec4f-/-
(f)
MFI
(g)
staining control
WT
Clec4f-/-
control
infected
KC
Non-KC CD11b+ cells
PNA binding
F4/80